Technische Universität Braunschweig

UNIVERSITÀ DEGLI STUDI FIRENZE

Study of New Processes to Obtain Aluminum Coatings by First Generation Ionic Liquids, for the Protection from Corrosion

Dissertation

submitted to and approved by the

Department of Life Sciences
University of Braunschweig – Institute of Technology

and the

Department of Civil and Environmental Engineering
University of Florence

in candidacy for the degree of a

Doktorin der Naturwissenschaften (Dr. rer. nat.) /
Dottore di Ricerca in Processes, Materials and Constructions in Civil and Environmental Engineering and for the Protection of the Historic-Monumental Heritage *)

by

Licia Barchi
Born 23.12.1979
from Cesena (Italy)

Submitted on	March 19th 2014
Oral examination on	May 7th 2014
1. Referent:	Prof. Claus-Peter Klages
2. Referent:	Prof. Ugo Bardi
3.Referent:	Prof. Uwe Schröder

2015

*) Either the German or the Italian form of the title may be used.

Index.

1 Introduction.

Ionic liquids (ILs), the object of this research project, are a particular class of ionic compounds which show lower melting points than the usual ionic compounds. By definition, ILs have melting points under 100 °C and in some cases even lower than 0 °C. The reason of this peculiar behavior is the size and the strongly asymmetric structure of the organic cations. However, this is not the only important characteristic of ionic liquids, which normally show the following properties:

- ✓ Low vapor pressure
- ✓ Wide electrochemical window
- ✓ Excellent thermal and chemical stability
- ✓ High electric conductivity
- ✓ Non flammability
- ✓ Low toxicity

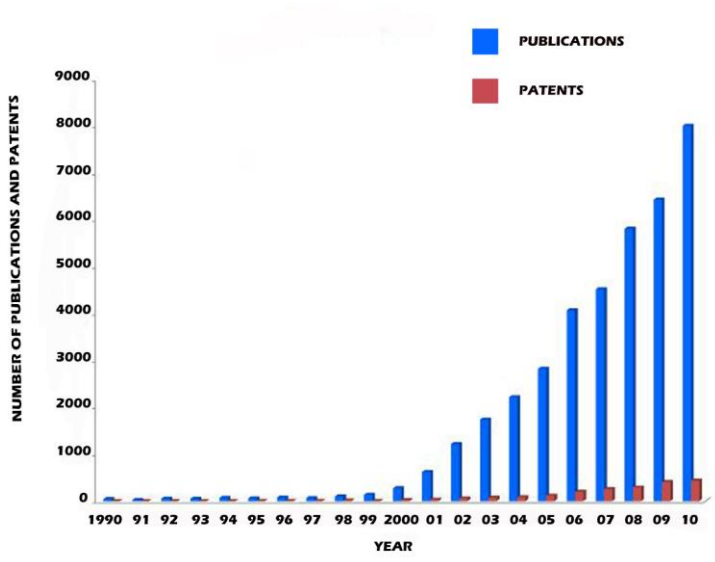

Figure 1 SciFinder search result for the keywords "ionic liquid" and "ionic liquids" up to Dec 2010, [1].

Because of such properties, these compounds are ideal candidates for a multiplicity of scientific and technological applications. In the last years an even larger number of scientific

papers focused on this subject. Figure 1 shows the number of publications concerning ionic liquids from 1990 to 2010, as determined by SciFinder [1].

The list of applications of ionic liquids keeps growing because of the fast development of new areas where they can be employed. Here, these fields will be considered:

- ✓ Solvents for organic reactions [2], [3]
- ✓ Biomaterials synthesis and extraction, by catalysis [4], [5], [6], [7]
- ✓ Electrolytes [8]
- ✓ Lubricants [9], [10], [11], [12], [13]

In the specific field of this work I focused on the excellent chemical and electrical properties of these substances (such as high electric conductivity, wide electrochemical window and thermal and chemical stability) which make ionic liquids the ideal mediums to conduct galvanic processes. In particular, the subject of the present work is related to aluminum electrodeposition and to a new approach to the creation of aluminum layers based on electroless deposition. In both cases ionic liquids were used as solvents.

The electrodeposition of aluminum from nonaqueous solvents has a long history and several attempts were made to bypass the limited electrochemical window of water in order to be able to produce aluminum films using galvanic processes. However, these attempts had no success for industrial applications because of various problems, including the toxicity and flammability of the solvents used. At the beginning of the 1980s a new approach took hold and led to systematic studies performed on the electrodeposition of aluminum from aluminum chloride ($AlCl_3$) based ionic liquids. Several kinds of ionic liquids have been reported in the literature as electrolytes for the electrodeposition of aluminum [14], [15], [16], [17]. These attempts do not yet have industrial applications, but show great promise in their capability of combining nontoxic and nonflammable solvents with the widespread need of the industry to create aluminum and aluminum alloy coatings, used for their corrosion resistance and ability of protecting substrates from high-temperature oxidation.

This thesis was dedicated to a study of aluminum deposition using ionic liquids as solvent and it was organized along three different lines of research:

1. Study of deposition of nanocrystalline aluminum layers using organic precursors in order to control the grain size;
2. Aluminum-silicon coatings as potential substitutes of traditional coatings;
3. Electroless plating of aluminum.

Study of deposition of nanocrystalline aluminum layers using organic precursors in order to control the grain size

The aim of this approach is to create nanocrystalline aluminum deposits on iron substrates by addition of different organic compounds to the plating bath as nucleation controllers. Nanocrystalline materials are particular interesting, because their mechanical properties are very often superior to those of conventional polycrystalline materials. Thanks to their small grain size, a large percentage of the atoms is located at grain boundaries and that confers special properties to the coating, such as increased strength and hardness as well as enhanced mass diffusivity, improved ductility/toughness, reduced density and elastic modulus, higher electrical resistivity, higher thermal expansion coefficient, lower thermal conductivity, and superior soft magnetic properties in comparison to polycrystalline materials [18]. The control of the nanostructure of the coating during electrodeposition can be obtained by suitable precursors which usually act by preferentially adsorbing on specific sites of the substrate. These precursors are usually organic compounds. The ones which were tested during the present work are: glutaric acid, 1-methoxy naphthalene, 2-chloro nicotinic acid, poly(ethylene glycol) methyl ether, glycolic acid, 2-pyridine sulfonic acid. An electrochemical investigation by cyclic voltammetry and constant potential depositions will be carried out at 25 °C and 100 °C. In this section of the project, I also tested an innovative approach to produce nanocrystalline Al coatings outside a dry box.

Aluminum-silicon coatings as potential substitute of traditional coatings in the gas turbine protection from corrosion;

The main target of this approach aims to find cost-effective and environmentally friendly technologies to protect the hot parts of industrial gas turbines against corrosion and high temperature oxidation. As the present state of the art, these parts may be covered with

several different kinds of coatings, each designed to improve the alloy resistance under specific working conditions. The most used technology in this field is the chromatization process, consisting in forming a chromate layer over the steel part by a reaction occurring at the interface. This technique is simple and cheap but it is becoming more and more unacceptable from an environmental point of view because of the presence of chromium (VI) in the waste products. Hence, there follows the interest in developing techniques which do not use harmful materials. The aim of this line of research is to obtain Al-Si alloys by electrodeposition from a ionic liquid containing Si metallic particles dispersed in the solution. These particles can be embedded in the aluminum matrix during electrodeposition to form a strong composite layer. A systematic study was conducted in terms of concentration and grain size of silicon particles in the electrochemical bath, stirring speed for homogenizing the suspension and deposition potential in order to control silicon percentage in the aluminum layer.

Electroless aluminum plating.

The purpose of this third line of research focuses on the possibility to obtain aluminum coatings using electroless plating, where the aluminum reduction process occurs without supplying an external current. This technique examines the possibility to obtain aluminum layers by thermal decomposition of $LiAlH_4$. The study reported here is still somewhat preliminary as it is mainly limited to the investigation of the solubility of $LiAlH_4$ powder and $LiAlH_4$ 1.0 M in diethylether in seven different ionic liquids. However, a series of isothermal experiments have been carried out in order to investigate the decomposition of the dissolved aluminum. These results indicate that it is possible to generate a metallic aluminum precipitate from these solutions and this result opens up the possibility of the electroless deposition of aluminum, a technology that, if developed at the industrial level, has enormous potential benefit in the fact that it can be used to coat parts which are impossible to coat by electrodeposition processes, such as the inside of tubes, convex parts, or parts having complex shapes and different curvature radii.

STATE OF THE ART.

2 Ionic liquids.

2.1 History of ionic liquids.

The term “Ionic liquid” (IL) indicates substances containing solely ions and that are liquid at relatively low temperatures. The standard definition, currently used, was created by Endres [19] and it establishes their melting point below 100 °C, but in many cases the melting point is even below room temperature. The history of ionic liquids started in 1914, when ethylammonium nitrate, $[EtNH_3]$ $[NO_3]$, was synthesized by Walden [20]. At the time, nobody had any idea of the concept of ionic liquid and for this reason no great attention was paid to the potential of this class of materials. Only a few studies were focused on these compounds until the mid-fifties, when Hurley and Wier reported that a mixture of N-ethylpyridinium bromide (EtPyBr) and $AlCl_3$ became liquid at unusually low temperatures and it could be used as electrolyte for the electrodeposition of aluminium [21], [22]. They investigated this system, but its use was limited because it is liquid only for a specific molar fraction of $X(AlCl_3)$ = 0.66 and is electrochemically unstable. Nevertheless, following this breakthrough in aluminum electrodeposition, many studies in the field were focused on ionic liquids. In 1978 Osteryoung and co-workers synthesized N-butylpyridinium chloride (EtBuCl) and they found that the anodic limit had improved changing from bromide to chloride [23]. Moreover, this compound is liquid at room temperature for a wider composition range of the mixture ($X(AlCl_3)$ = 0.66 – 0.43).

ILs composed of cations like dialkylimidazolium and alkylpyridinium derivatives and anions like chloroaluminate, have been the first class of these compounds with widespread utilization and constitute the so-called *first generation of ILs*. These ILs are mainly employed in the study of aluminum electrodeposition, but this generation of ionic liquids is moisture sensitive, due to the hygroscopic nature of $AlCl_3$, thus they can only be handled under inert-gas atmosphere. ILs have been extensively studied, following the works of Osteryoung and due to unique and accessible physical properties, such as thermal stability and low volatility,

a systematic research on the application of chloroaluminate ionic liquids as solvent was performed in the 1980s. Regardless of the handling difficulty of these ILs, because of their hygroscopic nature, they are still widely used in both organic and electrochemical fields [24]. In organic chemistry they are employed for syntheses where acid catalysts are needed at a high concentrations. Some examples of organic syntheses that can be carried out using first generation ILs as media are:

- ✓ Friedel-Crafts acylation and alkylation [25.]
- ✓ Alkane alkylations with alkenes [26].
- ✓ Diels-Alder reactions [27]
- ✓ Ziegler-Natta polymerization of ethylene [28].

During the last decade, an increasing number of new ILs have been prepared and used as solvents and the research was directed towards the synthesis of air and water-stable ILs, the *second generation of ILs.* In the 1990s new ionic liquids pertaining to the second generation were described, often based on 1,3 ethylmethylimidazolium cation and tetrafluoroborate anion, resistant to moisture [29]. In the literature there are review articles dedicated to room-temperature ionic liquids (RTILs) [30], [31], including application of non-chloroaluminates RTILs in electrochemistry [32]. These ILs normally consist of a large organic cation and an inorganic anion. One of the disadvantages of these ILs is the high cost, due to the cost of the starting materials and to the cost of the purification of final product required in the preparation. The most important disadvantage of the second generation of ILs is their toxicity, similar to those of chlorinated and aromatic solvents. However, this generation of ionic liquids is today the most studied by the scientific community owing to large possible combination of various cations and anions, which makes the number of imaginable ionic liquids virtually unlimited.

These ILs present interesting properties such as high viscosity, low melting point, different solubility in classic organic solvents, etc. Because of these properties, they have potential application such as energy materials, lubricants and even in the pharmaceutical field [33]. In the 2000s, Davis introduced the idea to incorporate a functional group in the anion or cation or both constituting ionic liquid, in order to to confer it particularly physical or chemical properties [34]. This new class of ionic liquids is called *third generation of ILs* and they are

applied mainly in the biological field. Since this generation is recent, only a few works have been published and commercialization is not expected to be obtained soon.

2.2 Characteristics of ILs.

Ionic liquids are usually composed of large and asymmetric organic cations combined with organic or inorganic anions. Large ions with a low degree of symmetry tend to reduce the lattice energy of the crystalline form of the salt and hence lower the melting point.

ILs are divided in two main categories:

1. simple salts made of a single cation and anion, for example [$EtNH_3$] [NO_3] (Figure 2)
2. binary ionic liquids where an equilibrium is involved, for example [BMIm]Cl [$AlCl_3$] (Figure 3)

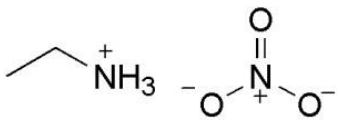

Figure 3 Structural formula [$EtNH_3$] [NO_3].

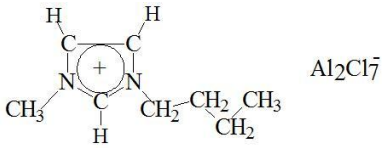

Figure 2 Structural formula of [BMIm]Cl [$Al_2Cl_7^-$].

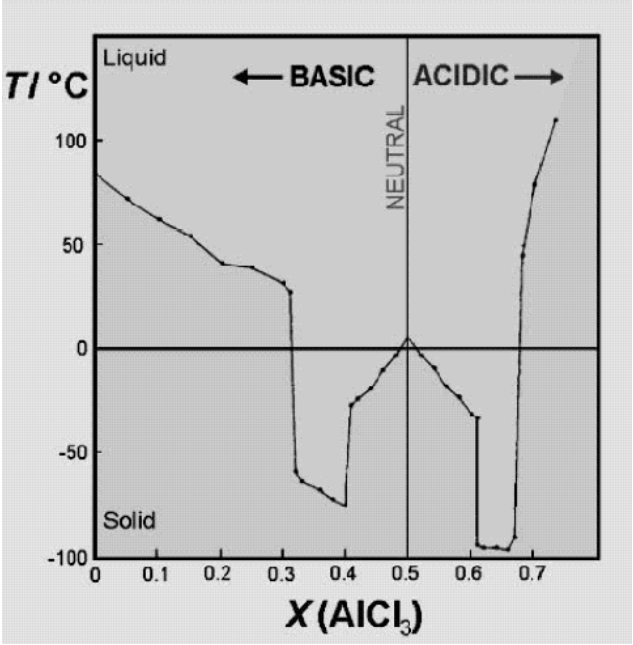

Figure 4 The phase diagram for mixtures of [EMIm[Cl and $AlCl_3$, [35].

Figure 4 [35], shows the melting point dependence on the relative fraction of the two species for the binary ionic liquid formed by [EMIm]Cl reacting $AlCl_3$. This reaction forms various anion species as the result of the acid/base character (in a Lewis sense) of the reactants. The mole fraction of these anions changes as a result of the initial relative amounts of neutral species mixed to form the IL. Compositions with an excess of [EMIm]Cl (i.e. $X(AlCl_3) < 0.5$) are called basic, those with an excess $AlCl_3$ (i.e. $X(AlCl_3) > 0.5$ are called acid and when $AlCl_3$ molar fraction is exactly 0.5 are called neutral. Depending on the mole fraction of $AlCl_3$ and [EMIm]Cl in the mixture, the melting point of the compound changes and it is evident in the graph that the lowest melting points are reached when $X(AlCl_3)$ is equal to about 0.33 and 0.66.

Moreover, even the distribution of the chloroaluminated anions depends on the mole fraction of $AlCl_3$ in the mixture. In fact, in alkaline environment the predominant species is the anion $AlCl_4^-$, whereas in acidic environment the anion $AlCl_7^-$, as shown in the Figure 5 [36].

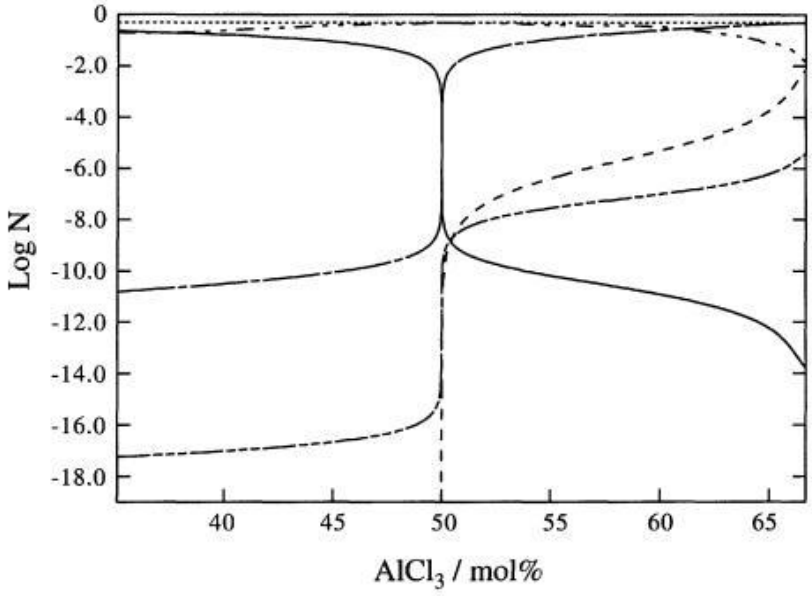

Figure 5 Distribution of the chloroaluminated anion (logarithmic scale) versus the molar fraction of $AlCl_3$ (in %) at 60 °C,[36]
__ : Cl^- ; _ . _ : $Al_2Cl_7^-$; _ . . _ : $AlCl_4^-$; _ _ _ : Al_2Cl_6 ; _ . . . _ : $AlCl_3$;

The distribution of the ionic species is very important with respect to electrochemical properties because polynuclear complexes are reduced more easily than mononuclear complexes. In the mononuclear species, for every aluminum atom there are four chlorine atoms, whereas in the polynuclear ones the average number of chlorine atoms is lower, and it produces a lower coordination energy.

The main physico-chemical properties of ILs of interest in relation to electrodeposition studies are:

- ✓ Conductivity
- ✓ Vapor pressure
- ✓ Temperature range of liquid state
- ✓ Hygroscopicity
- ✓ Viscosity
- ✓ Solvation power
- ✓ Electrochemical window

In the following paragraphs, these properties will be examined in order to describe the tendencies and the characteristics of this class of compounds.

2.2.1 Conductivity.

Conductivity is one of the most important properties of ionic liquids. In 1983, before the current definition of ionic liquids [19], Tissot gave a definition of the term "ionic liquid" that included conductivity. According to Tissot, a ionic liquid is any molten salt with a specific conductivity (σ) > 10^{-4} S cm^{-1}. Actually, the specific conductivity of the most common ILs is much higher than the threshold chosen by Tissot, as it is possible to observe in Table 1 where the values of the specific conductivity of the most common ionic liquids are reported [37], [38].

Ionic Liquid	**Conductivity (mS cm^{-1})**
[EMIm] [BF_4]	14
[BMIm] [BF_4]	3.5
[EMIm] [CF_3SO_3]	8.6
[BMIm] [CF_3SO_3]	3.7
[EMIm] [Al_2Cl_7]	15
[BMIm] [Al_2Cl_7]	9.2
[Bupy] [BF_4]	1.9

Table 1 Specific conductivity of ionic liquids, measured at 25 °C, [37], [38].

However, in comparison to conventional aqueous electrolyte solutions applied in electrochemistry, even the highest ionic liquid conductivity is much lower. For example, the specific conductivity of the aqueous KOH (29.4 wt.%) solution used in alkaline batteries is 540 mS cm^{-1}. This lower conductivity is a disadvantage in many electrochemistry applications; only partially compensated by positive factors related ionic liquids. A more fair comparison of electrolytes conductivity is between ionic liquids and other non-aqueous solutions and, in this case, ionic liquids show about one order of magnitude higher conductivity.

In general, conductivity is closely related to vapor pressure, which is an indication of the degree of intermolecular attraction in the compound: the strong anion–cation interaction in these Coulomb fluids is reflected in their extremely low vapor pressures and high conductivity. The conductivity is also related to viscosity (η). Considering the molar conductivity Λ and the electrolyte concentration c:

$$\Lambda = \frac{\sigma}{c}$$

$$c = \frac{n}{V}$$

where n is the number of moles of the charge carrier and V is electrolyte volume.

According to the Nernst-Einstein equation, in electrolyte solutions, molar conductivity is related to its diffusion coefficient (D):

$$\Lambda = \frac{z^2 e_o F D}{k_B T} = \frac{z^2 N_A {e_o}^2 D}{K_B T}$$

where z represents the valence of the charge carrier, e_o the elementary charge, N_A the Avogadro number, k_B the Boltzmann constant and F the Faraday constant.

On the other hand, according to the Stokes-Einstein equation, the diffusion coefficient D of a model spherical species of an effective radius (r) depends on the medium viscosity (η):

$$D = \frac{k_B T}{6\pi r \eta}$$

So, combining the 2 equations the following equation is obtained:

$$\sigma = \frac{z^2 {e_o}^2 N}{6V\pi r \eta}$$

Hence, the conductivity σ of a classical electrolyte solution is proportional to the number of charge carriers N and inversely proportional to the medium viscosity, η.

2.2.2 Vapor pressure.

As mentioned before, as a consequence of their strong anion–cation interaction, ILs show a low vapor pressure, close to zero and rarely even measurable. This characteristic is a remarkable advantage to reduce pollution, so it makes these compounds an environmentally friendly alternative to volatile organic solvents (VOCs) that are used for many industrial applications, such as synthesis, extraction and plating processes.

2.2.3 Temperature range of liquid state.

Ionic liquids show a wide temperature range in the liquid state. In most cases their melting point is lower, equal or just slightly higher than room temperature, whereas the thermal decomposition process starts at a temperature on the order of 300 °C-400 °C. Thanks to this property, it is possible to carry out deposition processes at temperature higher than 100 °C, in order to get higher values of the current density and to promote surface diffusion processes. Observed temperatures of solidification (freezing), melting and decomposition of some salts are show in the Table 2 [39].

Ionic Liquid	Solidification temp. (°C)	Melting temp. (°C)	Decomposition temp. (C°)
[EMIm] [BF_4]	-63	11	450
[EMIm] [Cl]	33	89	281
[EMIm] [PF_6]	5	62	481
[BMIm] [Br]	30	79	311
[EMIm] [I]	39	79	310

Table 2 Solidification, melting and decomposition points of some ionic liquids, [39].

As shown in the table, many ionic liquids show different values of melting and solidification temperature, a phenomenon due to supercooling. This phenomenon is related to the structure of an ionic liquid. The big size of the ions kinetically impedes the solidification process and it is the main factor that influences the gap between solidification and melting point. As a consequence, the solid can be obtained in an amorphous state at a lower temperature than the melting point. Regarding the decomposition temperature, the stability of the ionic liquid depends on the tendency to form a stable alkyl-X species. As can be seen in Table 2, the decomposition temperatures change with anion type and follow the order Cl^- > $[BF_4]^-$ > $[PF_6]^-$. So, ionic liquids more stable to high temperature decomposition, are ionic liquids containing weakly coordination anions.

2.2.4 Hygroscopicity.

The hygroscopicity of ILs has been widely studied because the presence of water can affect properties such as polarity, viscosity and conductivity. Water can also react with constituents of the ILs with adverse effects. Imidazolium halide ionic liquids, for example, are extremely hygroscopic, and for this reason it is difficult to make completely proton-free

chloroaluminate ionic liquids. As already reported, first generation ionic liquids are particularly hygroscopic, so their use is restricted in organic processes or they have to be handled under a dry atmosphere. Second generation ionic liquids are usually classified as hydrophobic, but can absorb water from the atmosphere, for example [BMIm] [NTf_2] saturates with about 1.4 mass% of water.

2.2.5 Viscosity.

Generally, ILs are much more viscous than conventional organic solvents, and the viscosity values of most ILs are 2–3 orders of magnitude larger than those of organic solvents. Evidently, high viscosity will increase the number of problems in chemical processing, as handling (dissolution, decantation, filtration, etc.) or reduction of mass-transfer rate in reactions. On the other hand, some applications are favored by highly viscosity, such as stationary phases for gas-liquid chromatography and when ILs are used as lubricants. Therefore, many studies were focused on the viscosity of ionic liquids in order to understand the relationship between viscosity and ionic structure. ILs viscosity is related to the cation–anion pairing and their structural characteristics such as cationic size, length of substituted group, anionic size, and anionic shape [40], [41], [42]. In addition, some theoretical studies using modeling and simulation were performed for ILs viscosity to describe the dependence of viscosity on temperature and, in consequence, on pressure [43]. The correlation between viscosity and conductivity has been also discussed in paragraph 2.1.1.

2.2.6 Solvation power.

One of the most important properties of ILs is their ability to dissolve both ionic and covalent compounds. This peculiarity makes ionic liquids attractive not solely as solvents, but also for the extraction of materials from solutions. Their solvation power depends on several factors, but the most remarkable ones are their polarity and the coordination ability of their ions. Ionic liquids are similar to dipolar, aprotic solvents and short-chain alcohols, but depending

on the constituting anions the polarity can be changed. From an electrochemical point of view, such a wide solvation power allows to dissolve in the electrochemical bath both inorganic salts and organic additives, that can be useful to modify the growth mechanism of deposits.

2.2.7 Electrochemical window.

The electrochemical window is the range of voltages over which the solvent is electrochemically inert. It depends on the tendency of the cation to be reduced and of the anion to be oxidized. In relation to the purposes of the present study, this is one of the most important properties we can take advantage of by using ILs as solvents. Pure water has a thermodynamic stability of only 1.23 V. In fact electrolysis of water into oxygen and hydrogen(e.g. the decomposition) occurs by redox reaction:

$2H_2O \rightarrow O_2 + 4H^+ + 4e^-$ $\quad E^o_{red} = 1.23V$

$2H^+ + 2e^- \rightarrow H_2$ $\quad E^o_{red} = 0.00V$ (this is hydrogen's standard electrode potential that is defined zero, in order to calculate all other electrode reactions by comparison)

So it is not possible to reduce ions of less noble metals such aluminum and alkali metals. ILs, however, show a larger electrochemical window, and that allows the reduction and the electroplating of aluminum and other electropositive metals.

The measurements of electrochemical stability depend on applied reference electrodes. To compare the data it is necessary to use the same reference system and that should be strictly electrochemically defined, while also the redox couple determining the potential has to be defined. In Table 3 some literature data about the electrochemical windows of some ILs are reported [37]. These measurements were performed using as working electrode platinum and as reference electrode Ag/Ag^+ (0,01 mol dm^{-3} in DMSO). The stability windows are reported to be in a broad range from 2.2 to 4.6 V , but in the literature some cases are reported where it can reach even value as large as 6.0 V [44].

Ionic liquid	Electrochemical window (V)
[EMIm][BF_4]	2.6
[EMIm][NTf_2]	4.5
[BMIm][Br]	2.2
[BMIm][BF_4]	4.2
[BMIm][PF_6]	4.4
[BMIm][NTf_2]	4.6

Table 3 Electrochemical windows of some ILs. The measurements are performed using as working electrode platinum and as reference electrode Ag/Ag^+ 0.01mol dm^{-3}in DMSO, [37].

In several papers, a comparison of the electrochemical stability of different ILs was studied and a trend in the electrochemical stabilities of the types of ionic liquid cations was found as follows: pyridinium < pyrazolium < imidazolium< sulfonium < ammonium. Overall, the quaternary ammonium-based ionic liquids are the potential window champs. Regarding the anion stabilities towards oxidation appear to follow the order: halides (Cl^-, F^-, Br^-) < chloroaluminates ($[AlCl_4]^-$, $[Al_2Cl_7]^-$) < fluorinated ions ($[BF_4]^-$, $[PF_6]^-$, $[AsF_6]^-$) < triflate/triflyl ions ($[CF_3SO_3]^-$, $[(CF_3SO_2)_2N]^-$, $[(C_2F_5SO_2)_2N]^-$, $[(CF_3SO_2)_3C]^-$). In general, the most common stability window of ILs is around 4.5 V [38].

3 Electrochemical cell.

The electrochemical cell is where the redox reactions take place. Depending on the kind of reaction, the cells are classified as:

- ✓ Galvanic or voltaic cells are systems where a spontaneous reaction occurs.
- ✓ Electrolytic cells are systems where reactions occur by an applied electrical potential.

Electroplating processes occur only in electrolytic cells, so this section will be mainly focused on working principles of this type of electrochemical cell.

An electrochemical cells consists of at least two electrodes and an electrolyte. The electrolyte is a solid or liquid ionic conductor which allows the electrical contact between the electrodes. The electrodes are solid conductors, usually metals, where the oxidation and reduction reactions occur. Oxidation occurs at the electrode termed the anode, the reduction occurs at the electrode called the cathode and the electrons flow from anode to cathode [45].

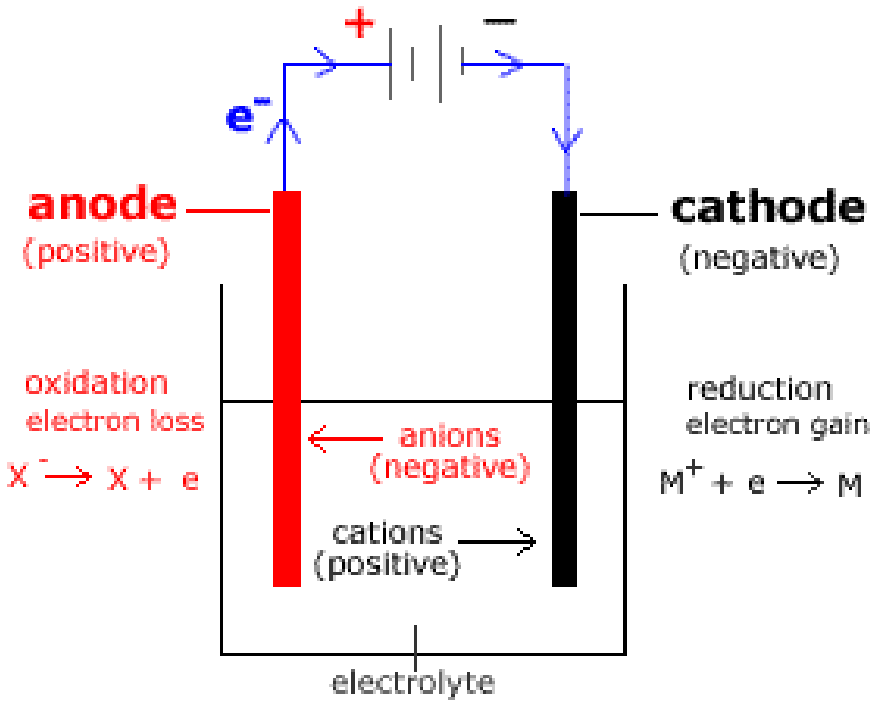

Figure 6 Scheme of an electrolytic cell [45].

3.1 Cell potentials and thermodynamics.

The preferred direction of a reaction in an electrochemical cell can be determined using the Gibbs free energy (ΔG), as it can be done for the traditional, non electrochemical reactions:

$\Delta G < 0$ reaction is spontaneous, thermodynamically downhill.
$\Delta G > 0$ reaction is nonspontaneous, it proceeds in reverse direction.
$\Delta G = 0$ equilibrium, no reaction takes place.

In an electrochemical system, the direction of the reaction is determined by the electromotive force (E_{cell}), which is related to Gibbs free energy by the equation:

$$\nu F E_{cell} = -\Delta G$$

where:

ν is number of electrons exchanged in the reaction.
F is the charge of 1 mole of electrons (Faraday constant).
E_{cell} is the electromotive force of the cell.
ΔG is the free energy of the reaction.

So, the reaction will be spontaneous when the electromotive force E_{cell} in the cell is positive, and it will be spontaneous, but in the opposite direction, when E_{cell} is negative.

$E_{cell} = 0$ means that the cell is at equilibrium.

To determine the value of the electromotive force it is necessary to introduce the Nernst equation which relates the potential of a half-cell to the standard half-cell potential and activity of the reactions and species in the cell.

For example, cathode potential can be determined using the following equation, and the same can be done for the anode potential:

$$E_{cathode} = E^{0}_{cathode} - \left(\frac{RT}{zF}\right)\ln\left(\frac{a_{red}}{a_{ox}}\right)$$

where:

ν is number of electrons exchanged in the reaction

F is the charge of one mole of electrons (Faraday constant)

$E_{cathode}$ is the half-cell potential

a_{red} is the activity of the reduced species

a_{ox} is the activity of the oxide species

$E^{0}_{cathode}$ is the standard half-cell potential

R is the ideal gas constant

T is the temperature in Kelvin

In this way electromotive force of the cell can be calculated by subtraction of half-cell potentials:

$$E_{cell} = E_{cathode} - E_{anode}.$$

3.2 Electrical double layer.

The electrical double layer is a structure that appears at the interface formed by electrode and electrolyte. It is due to the presence of an electrical charge on the electrode surface that is not transferred to the solution. This charge attracts the ions with opposite charge in the electrolyte and it collects them on the electrode surface. So, the electrode is surrounded by two parallel layers of charge.

Helmholtz's model assumes that there are only electrostatic interactions between the electrode surface and the ions in the electrolyte and no electron transfer reactions occur at the electrode. Because the electrode holds a charge Q, in order to balance this charge and keep the neutrality, ions present in the solution, with opposite charge, are attracted to the interface electrode/solution.

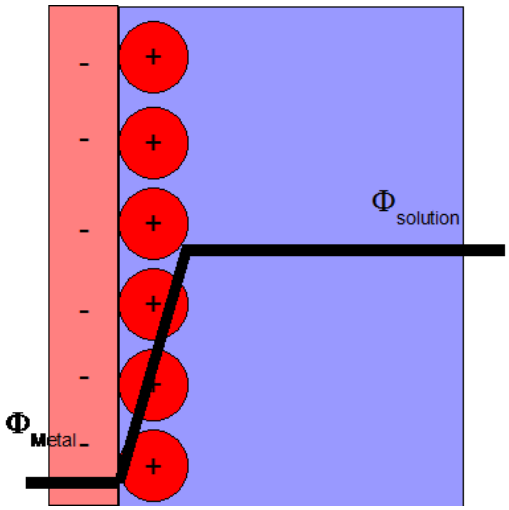

Figure 7 Scheme of Helmholtz's electrical double layer [47].

The model assumes they form a layer in front of the electrode surface, determining a double layer with opposite charge which causes a potential drop [46].

On the basis of this point of view, electrical double layer is similar to an electrical capacitor where charged plates are separated by the distance D. In the double layer model D is the distance between the electrode surface and the first ion layer (Figure 7) [47]. This model is a simple idea about the system; later different and more sophisticated models were proposed, such as Stern's model, anyway Helmhotz's model is sufficient to understand that when electrical signal is apply to an electrochemical cell, it is necessary to consider this phenomenon.

3.3 Electrochemical kinetics.

The previous considerations regard the thermodynamic aspects of an electrochemical process and they are valid only at the equilibrium conditions. However, electrochemical reactions are controlled by kinetics factors which strongly influence the rate of chemical reactions and that determines whether they occur or not. In order to understand the kinetics behaviour of an electrochemical reaction it is necessary to study the phenomena occurring on the interface electrode/electrolyte. Assuming that charges do not transfer across the interface, when we apply a potential at the electrode charge accumulation of opposite sign results on electrode surface. The ions held on to electrode surface are distributed as reported in the previous paragraph. The electrochemical reaction rate is mainly controlled by two phenomena:

1) Electron-transfer reaction between metal and ions in solution.
2) Mass transport from and to electrodes.

3.3.1 Electron Transfer.

The potential of an electrode measures the energy of the constituent electrons. More negative potentials allow electrons to reach higher energy levels. At sufficiently negative potentials, the electrons achieve a sufficient energy to permit electron transfer from the electrode to solution if it is possible to obtain a chemical reaction with a component of the solution. Suppose that, at an applied potential, the following reaction occurs at the metal electrode surface:

$$O + e^- \underset{k_O}{\overset{k_R}{\rightleftharpoons}} R$$

That is, electrons from the electrode are received by species O at the metal/solution interface, and the reaction yields a product R. This electron transfer constitutes current flow. So, the current flow is related with the O/R reaction, a quantitative relationship exists

between reaction rate and current. The current flowing in either the reductive or oxidative direction can be predicted using the following expressions:

$$i_a = nFAk_o C_R$$

$$i_c = -nFAk_R C_O$$

In these equations i_c is the current flowing for the reduction reaction and it is related to the electrode area (A), to the concentration of the reactant on the electrode surface, C_O, to the rate constant for the electron transfer, k_R, and F is Faraday's constant. The same expression exists for the oxidation, but in this case the current is i_a, the concentration that of the reactant on the electrode surface is C_R, and the rate constant for electron transfer corresponds to that k_O. By definition the reductive current is negative and the oxidative positive, the different sign just indicates in which direction current flows. The constants k_O and k_R are influenced by the applied voltage and it is explained by transition state theory where the reaction is considered to occur via an energy barrier and the transition state corresponds to the top of this barrier.
For a simple chemical reaction, as:

$$A \xrightarrow{k} B$$

The rate of the process is given by the equation:

$$k = Ze^{\frac{-\Delta G}{RT}}$$

where ΔG is the activation free energy. This condition is also valid for electrode reactions, where redox reactions occur, as that one reported at the beginning of the paragraph. In this case, the free energy plot is reported in the Figure 8.

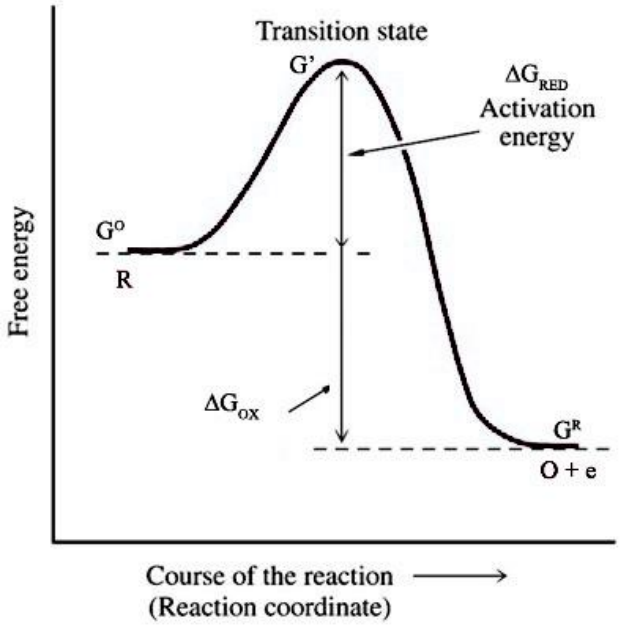

Figure 8 Free energy plot for redox reactions.

The activation free energy for the reduction and oxidation reactions are, respectively:

$\Delta G_{RED} = G' - G^O$

$\Delta G_{OX} = G' - G^R$

consequently, reaction rates k_{red} and k_{ox}, are given by:

$$k_{red} = Ze^{\frac{-\Delta G_{RED}}{RT}}$$

$$k_{ox} = Ze^{\frac{-\Delta G_{OX}}{RT}}$$

Applying different voltages, we will obtain different free energy plots, but the free energy of R will be invariant, whereas free energy value for O + e shows a strong dependence with voltage. This phenomena can be explained in terms of the Fermi level diagrams: applying a different voltage, the Fermi level increases (or decreases) and for this reason the energy state of the electrons changes. Moreover modifying voltage also the activation energy can be altered. So the rate constants, for the forward and reverse reactions, are altered by the applied voltage. In order to formulate a model, it has been assumed that the effect of voltage on the free energy change follows a linear relationship. Using this linear relationship,

it is possible to observe, using the Butler-Volmer model, that the activation free energies for reduction and oxidation vary as a function of the applied voltage (V):

$\Delta G_{RED} = \Delta G_{RED}$ (V=0) + αFV

$\Delta G_{OX} = \Delta G_{OX}$ (V=0) - (1-α)FV

The parameter α indicates the transfer coefficient and typically it has a value of 0.5. This factor provides an idea how the voltage influences the transition state The free energies ΔG_{RED} (V=0) and ΔG_{OX} (V=0) are the chemical component of the activation free energy change and they just depend on the chemical species [46]. The activation free energy terms written above can be substituted into the expressions for the oxidation and reduction rate constants, which gives:

$$k_{red} = Ze^{\frac{-\Delta G_{RED}^{V=0}}{RT}} e^{\frac{-\alpha FV}{RT}}$$

$$k_{ox} = Ze^{\frac{-\Delta G_{OX}^{V=0}}{RT}} e^{\frac{(1-\alpha)FV}{RT}}$$

As can be observed, for the electron transfer phenomena, rate constants are related to exponential of the applied voltage. That means changing the voltage it is possible to modify the rate of electrolysis reaction. One of the most important investigation technique, called voltammetry, is based on this principle.

Anyway, electrolysis reaction is not driven just by electron transfer kinetics, but even by the rate of transport to the electrode, which controls the whole reaction [47].

3.3.2 Mass transport.

In the previous section it has been explained that the reaction rate is related to electrode voltage by an exponential relationship. That means increasing the voltage the reaction rate

(i.e. the current) increases exponentially. In reality the amount of current which can pass in a electrochemical cell is not unlimited. In fact considering the current i_c :

$$i_c = -nFAk_R C_O$$

for a electrode area A, the reaction can be controlled by two parameters: the rate constant, k_{red} and the concentration of the reactant on the surface, C_O. A high value of rate constant means that reactants close to the electrode surface undergo immediately the reaction. In this condition the current i_c is controlled by the amount of new reactants arriving to the electrode surface from the bulk solution. Thus, in order to calculate the current flowing in the electrochemical cell, it is fundamental a knowledge of the movement of the reactants in the electrochemical bath [46].

Electrolysis reactions can be influenced by three different form of mass transport:

- Diffusion
- Convection
- Migration

Diffusion is a mass transport phenomena which depends on distribution of reactant and product concentration in the electrochemical bath. Because in the electrochemical cell the redox reaction occurs just at electrode/solution interface, in this area reactant concentration is lower than in bulk solution, whereas product concentration is higher. The forces that mainly drive diffusion process are entropic, that move the species in the solution, in order to obtain a more uniform distribution of the concentrations.

The rate of movement of mass by diffusion can be calculated by Fick's laws.

The first law is:

$$J_0 = -D_0 \left(\frac{\partial C_0}{\partial x} \right)$$

where J_0 is the diffusional flux (the rate of movement of mass by diffusion) and it is related to the concentration gradient and the diffusion coefficient Do. The equation has a negative sign because the material moves down a concentration gradient, from regions of high to low concentration. To see how the concentration of material varies as a function of time it is necessary to introduce Fick's second law, that can be derived from Fick's first law:

$$\frac{\partial C_0}{\partial t} = D_0 \left(\frac{\partial^2 C_0}{\partial x^2} \right)$$

On the left hand side is reported the rate of change of the concentration C_0 as a function of time (t). It is related to the change in the concentration gradient (in this case x is the direction normal to an electrode surface and it is the direction where diffusion is considered). So if the change in concentration is greater, then even the rate of diffusion is greater. In practice diffusion is often the most significant transport process for many electrolysis processes [46].

Convection is a mass transport that results from the action of a force on the solution, such as a pump, a flow of gas or gravity. Regarding electrochemical measurements the most important aspect of convection is natural convection. It could be present in any solution and usually it is due to small thermal or density differences and acts to mix the solution. Natural convection affects electrochemical experiments when the measure takes more than 20 seconds, but it could be easily avoided by stirring the solutions, e.g. by means of a magnetic bar mixing the solution, and reducing the diffusion layer it is possible to obtain faster deposition rates, [48].

The last form of mass transport considered is migration. Applying a voltage on the electrodes, any charged species present close to the electrode surface is attracted or repulsed by it, depending on their sign. The following equation describes the phenomena considering one-dimensional case:

$$J_m \propto -uC_0\left(\frac{\partial\phi}{\partial x}\right)$$

J_m is the current density caused by migration effect, u is the ions mobility, C_0 is the concentration of charged species and ϕ is the electric potential in the position x. The migratory flux is proportional to mobility constant of charged species, concentration of the charged species and electrostatic force that is caused by the ϕ gradient. Migration effect is difficult to predict, because of ion solvation effects and diffuse layer interactions in solution. In order to remove migratory effects, most voltammetric measurements are performed in solutions which contain an inert electrolyte that does not undergo electrolysis itself but protects the reactants from migratory effects. Moreover, the introduction of a background electrolyte can promote the passage of current through the solution.

4 Investigation techniques used in the present study.

In this section, the main investigation techniques employed in this study will be described. Most of these methods are well known in the field of chemistry and in this chapter the attention will be focused on their application in the ionic liquids/metal interface characterization.

Two principal techniques used here will be described:

- ✓ SURFACE AND NEAR-SURFACE ANALYSIS: Scanning electron microscope coupled with X-ray microanalysis (SEM and EDX).
- ✓ ELECTROCHEMISTRY TECHNIQUES: Cyclic voltammetry (CV).

4.1 Surface and near surface analysis.

4.1.1 Scanning electron microscope coupled with X-ray microanalysis.

A scanning electron microscope (SEM) can provide extremely detailed images of the surface under study, for this reason it is one of the most common analytical tools in near surface analysis. Coupling the SEM instrument with an energy dispersive X-ray spectroscopy detector (EDX), it is possible to identify elements of almost the entire periodic table. The SEM instrument is based on the generation of an electron beam by means of a hot filament, made of various types of materials. The most common is the tungsten hairpin gun, but other types of filament exist, such as lanthanum hexaboride (LaB_6) filaments and field emission guns. This filament functions as the cathode. It is heated by the Joule effect and a voltage is applied to it in order to extract electrons out of it. Electrons are then accelerated and focused by means of a series of electrodes located in the microscope column. The vertical path through the microscope followed by the electron beam is kept under vacuum in order not to obstruct the movement of the electrons. This beam is condensed by a condenser lens, and focused as a very fine point on the sample by the objective lens. Once the beam hits the sample, electrons and X-rays are ejected from the sample. Detectors collect these X-rays,

backscattered electrons and secondary electrons and convert them into a signal that is sent to a screen. This produces the final image. A scheme of the apparatus is reported in Figure 9 [49].

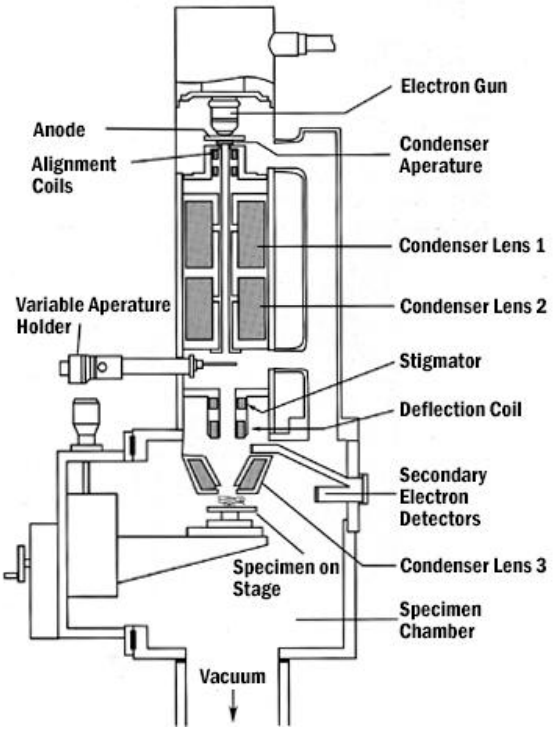

Figure 9 Scheme of the scanning electron microscope [49].

The depth of the analyzed area inside the specimen depends on the following factors:

- ✓ The atomic number of the material. Higher atomic number materials absorb or stop more electrons, so the interaction volume is smaller.
- ✓ Accelerating voltage used during the examination. Higher voltages penetrate deeper into the material and generate larger interaction volume.
- ✓ Angle of incidence for the electron beam. The greater the angle the smaller the volume.

An atom at rest contains ground state electrons (unexcited) in discrete energy levels or electron shell bound to the nucleus. When the incident beam hits an electron in an inner shell, the electron is excited and ejected from the shell. It causes the appearance of an electron hole, where the excited electron was. An electron from an outer higher energy shell can fill this hole and, in this case, the difference of energy between the higher energy shell

and the lower energy shell is released in the form of an X-ray photon. An energy dispersive spectrometer measures the number and the energy of the X-ray photons emitted from the sample. This allows the elemental composition of the sample; in fact the X-ray photon energies are characteristic of the difference in energy between the two shells and of the atomic structure of the element. EDX can determine the elemental composition of individual points or map out the lateral distribution of elements from selected areas.

4.2 Electrochemistry techniques.

4.2.1 Three electrode cell.

In the electrochemical cell different phenomena occur at the interface between the counter electrode (CE) and solution and between working electrode (WE) and solution. In order to characterize the effects which take place at the WE/solution interface it's necessary to separate them, adding a third electrode called reference electrode (RE). This reference electrode allows to measure the potential difference among the two electrodes, and that is possible because it conserves a constant potential and current does not pass through it [50]. The most used reference electrodes are saturated calomel electrode and silver chloride electrode, but using nonaqueous electrolytes it is not possible to employ this kind of reference electrodes. In this case (ionic liquids as electrolytes) quasi-reference electrodes are used (QRE). They are usually constituted by metallic wires, for example silver or platinum, directly immersed in the electrochemical bath. Their main characteristic is that their impedance is equal to zero, moreover they can keep a constant potential.

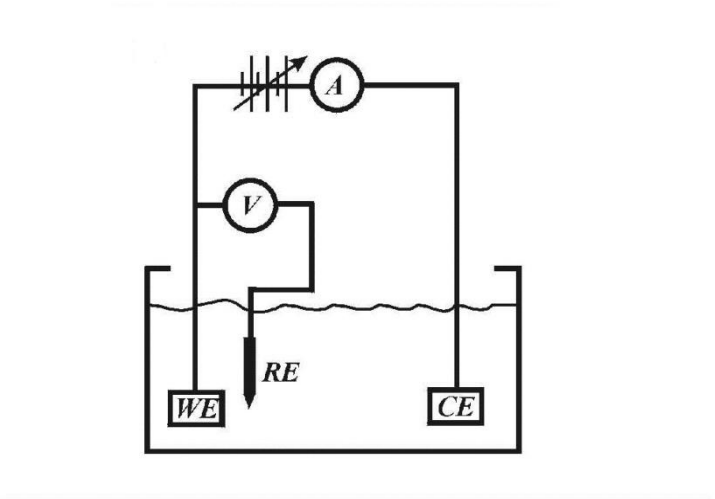

Figure 10 Schematic representation of the electrochemical cell used in this study. WE indicates the working electrode, RE the reference and CE the counter [50].

4.2.2 Potentiostat and galvanostat.

A three electrode cell needs to employ a particular instrument termed potentiostat which is used in most electrochemical measurements. Potentiostat can keep potential difference between the working electrode and reference electrode constant and corresponding to the value specified by the user. In this way, during the experiment, it measures and displays the current flow between working and counter electrodes. Modern potentiostats allow to apply not just a constant potential, but even several potential functions as triangular wave form showed in the Figure 12. A basic diagram of a potentiostat is presented in Figure 11.

Electrodeposition experiments are usually carried out using a constant current, not potential difference. In this case it's employed an instrument called galvanostat (in this case it is not necessary to employ the reference electrode). Nowadays both potentiostat and galvanostat are assembled in a unique instrument.

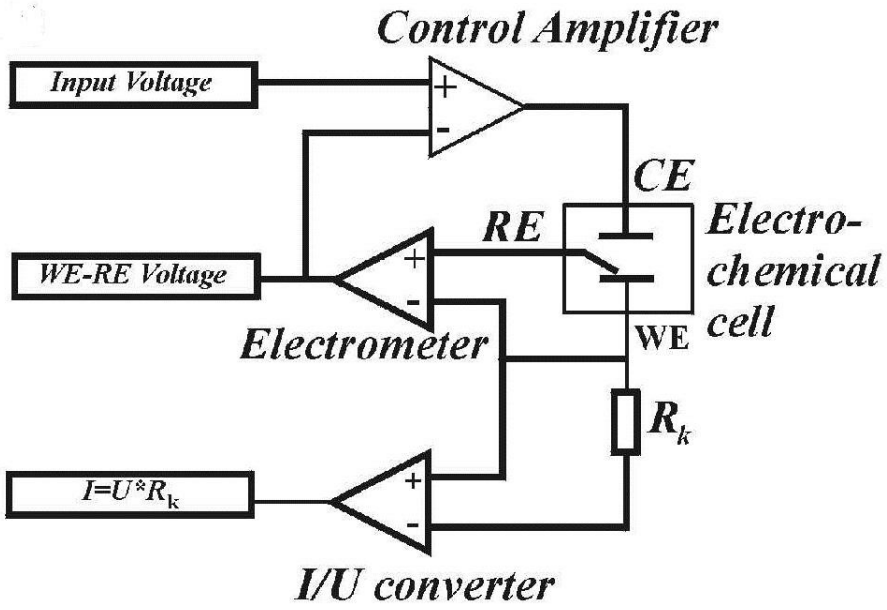

Figure 11 Basic potentiostat circuit [50].

4.2.3 Cyclic voltammetry (CV).

Electrochemical behavior of a system can be investigated measuring the current response due to the application of a potential between WE and RE. Cyclic voltammetry is a technique by which it is possible to monitored the current flowing through the counter electrode, while WE potential is scanned relative to the reference electrode. The current response (called Faradic) is a measure of the electron transfer which takes place when a oxidation or reduction occurs on the electrode surface [51]. So, in this way, the behavior of electroactive species present in the solution can be characterized. Usually CV is based on a triangular potential waveform; that is, the potential is changed as a linear function of time (see Figure 12 [52]).

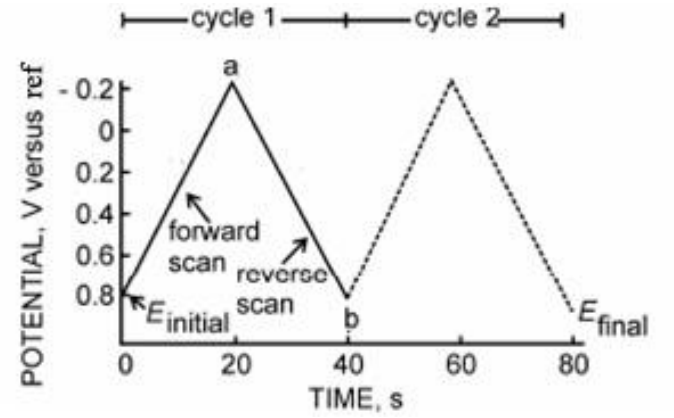

Figure 12 Potential wave form for cyclic voltammetry [52].

During the forward scan, when the potential applied on WE achieves more negative values than the reduction potential of redox couple present in the solution, this one undergoes a reduction. It induces an electron transfer denominated cathodic current. Similarly, during the return scan, when the potential applied on WE is more positive than the reduction potential of redox couple, it undergoes an oxidation and that induce a electron transfer in the opposite direction denominated anodic current. By IUPAC convention, anodic currents are defined positive and cathodic currents negative.

A typical voltammogram is shown in Figure 13 [51], where:

- E_i is initial positive potential,
- E_{switch}, is negative potential where the scan is reversed, The current is first observed to peak at
- E_{pc} is potential where is observed the first current peak (with value i_{pc}) and at this potential the reduction is occurring. After that the current decreases because of diminution of the oxidizing species from the diffusion layer.
- E_{pa} is potential where is observed the second current peak (with value i_{pa})) and at this potential the oxidation is occurring.

If the charge–transfer reaction is reversible, the ratio i_{pr}/i_{pf} will be equal to 1.0 (in Figure 13 $i_{pa} = i_{pr}$ and $i_{pc} = i_{pf}$).

In addition, for such a system it can be shown that:

1) Peak potentials E_{pa} and E_{pc} are independent of scan rate and concentration,

2) $(E_{pa} + E_{pc})/2$ is approximately equal to the formal potential for the redox reaction

3) $E_p = E_{pa} - E_{pc}$ is close to 59/n mV at all scan rates [51].

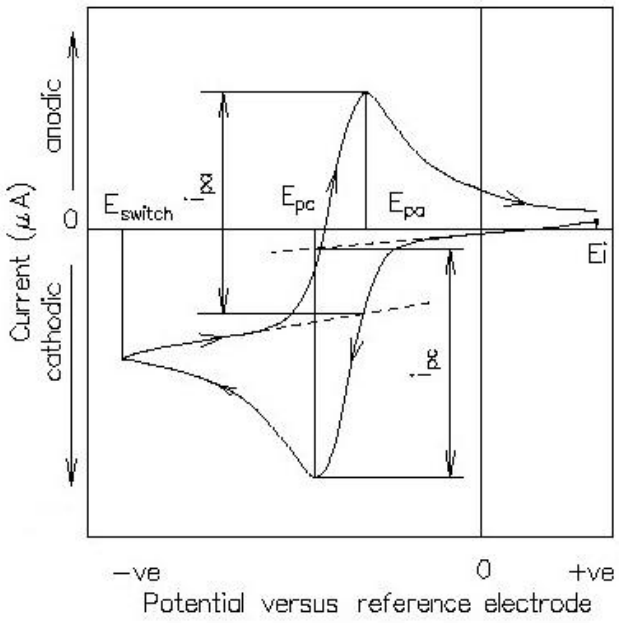

Figure 13 Typical cyclic voltammogram [51].

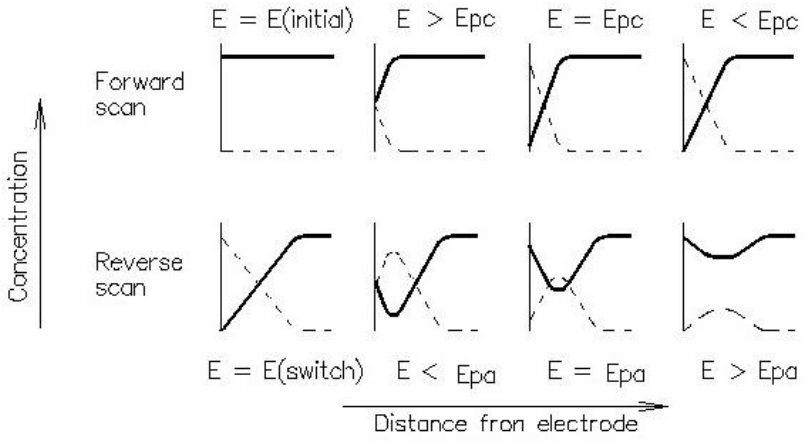

Figure 14 Diagrams showing concentration-distance profile at various phases of the cyclic voltammetry; the solid lines correspond to the oxidizing species and the dotted lines to the reducing species [51].

When all of these conditions are satisfied, the system can be assumed reversible, so they are good indicators about the reversibility of the redox reaction.

During the cyclic voltammetry experiment, the solution is kept unstirred, so the mass transport occurs only by diffusion that is due to the concentration gradient around electrode surface. In Figure 14 [51] are showed concentration-distance profile at different phases of cyclic voltammetry process.

Because recorded current, in a CV experiment, is strongly linked to these diffusional properties, it is related to several parameters. As demonstrated by Randles–Sevcik equation [51], the peak current for the forward sweep in a reversible system at 298 K is given by:

$$i_{pf} = \left(2,69 \times 10^5\right) n^{3/2} A D^{1/2} v^{1/2} C^*$$

where:

- n is the number of electron equivalent exchanged during the redox process
- A (cm^2) is the active area of WE
- D ($cm^2\ s^{-1}$) is the diffusion coefficient
- C^* ($mol\ cm^{-3}$) is the bulk concentration of the electro-active species
- v is the voltage scan rate ($V\ s^{-1}$)

5 Aluminum.

5.1 Characteristics and corrosion resistance.

Nowadays, aluminum and its alloys are widely studied in the engineering world, owing to their high-specific strength, low density, corrosion resistance, suitability for surface treatments, high thermal and electrical conductivity and common presence in the Earth's crust. This work is dedicated to the development of aluminum deposition processes, because of its excellent corrosion resistance and its capability of protecting the substrate from high temperature oxidation.

Aluminum is surprisingly resistant to corrosion considering its low electrode potential, equal to -1.68 V. Electropositive metals, as aluminum, are easy to oxidise. However, the kinetics of oxidation depends also on other factors. In oxidising media (air, water, etc.), aluminum spontaneously forms a uniform oxide layer on the surface, corresponding to the formula Al_2O_3. This layer rapidly becomes sufficiently thick to prevent further oxidation. On a freshly prepared clean aluminum surface the thickness of the air-formed film is about 2.5 nm, whereas on a several years old aluminum surface, it can reach 10 nm or more.

The oxide film is composed of two parts:

- The barrier layer is the inner layer, in contact with the metal. The name is due to its dielectric properties. It is compact and amorphous and it forms very quickly and, if damaged, it will reappear immediately, even in poorly aerated areas. The maximum thickness of this first layer is in the order of 4 nm.
- The second layer grows on the top of the first one and it is porous and less compact than the barrier layer. It reaches its final thickness after several weeks or even months. The formation rate depends on physicochemical conditions, as humidity and temperature.

Spontaneous aluminum corrosion resistance is limited to environments where the oxide layer is stable. The corrosion rate increases in environments with a pH higher than 9.0 (alkaline conditions) or lower than 7.0 (acidic conditions) or where aggressive ions (as Cl^-) are present. Moreover, in water, the rate of corrosion of aluminum depends on several parameters coupled to water: temperature, electric conductivity and others. It also depends

on the alloy composition, heat treatment and surface state. The composition, size and quantity of alloy constituents (such as Al_3Fe, $Al_6(Mn,Fe)$, $\alpha(FeSi)$ or pure silicon) affect the corrosion rate. If the corrosion potential of alloy constituents is different corrosion resistance is influenced. The most common process to improve aluminum corrosion resistance is anodizing in order to form a stable and controlled protective oxide layer. Setting the anodizing process parameters (potential/current, electrolyte type, etc.) and elemental composition of electrode, it is possible to determine oxide film properties and thickness and to enhance its corrosion resistance.

5.2 Aluminum deposition.

Aluminum electrodeposition was studied since the beginning of the 20th century. It is a more difficult process than conventional electrodeposition since it cannot be performed in acqueous baths owing to the limited electrochemical window of water compared to the strongly negative value of aluminum reduction standard potential (1.66 V). Therefore, electrodeposition of aluminum can only be performed in non-aqueous solvents which have a sufficiently large electrochemical window.

A variety of tests have been performed in the past using conventional organic solvents and investigations reported good yields and good quality of the deposits from benzene and toluene baths. Some practical industrial processes were proposed using these solvents as electrochemical baths, but they were abandoned because of the high toxicity and flammability of the baths. Some studies were performed on high temperature aluminum deposition from alkali chloroaluminate salts. In this case, it was possible to obtain not just aluminum coatings, but also binary alloys as Cr-Al [53], Mn-Al [54], Ni-Al [55] and Ti-Al [56]. However, the scale-up of the process met several problems, such as the use of high temperatures (>150 °C), aggressive salts and the elevated vapour pressure of the dimer Al_2Cl_6.

Non electrochemical techniques to deposit uniform aluminum films exist; for instance chemical vapour deposition (CVD), and physical vapour deposition (PVD), but they also present disadvantages. Chemical vapour deposition needs to be done on high temperature

substrates, which imply a consistent increase of production costs. Moreover it occurs by a complex process using toxic and corrosive gasses. Regarding physical vapour deposition, the process has been known for a long time. The problems related to it are that it is possible to deposit only in “line of sight” and that the obtained coatings have usually poor adhesion to the substrate. A further disadvantage of the method is the need of high vacuum, which requires expensive facilities.

Because of the problems described above, in the 1980s, studies started to focus on the possibility to obtain aluminum deposition from ILs. Several ionic liquids based on N-alkyl-pyridinium and di-alkyl-imidazolium cations were investigated, resulting very promising due to the high current supported [24], [57], [58] and [59]. In the solution composed by these ionic liquids, there occur the following equilibrium reactions:

$2\ AlCl_3 \rightarrow Al_2Cl_6$

$AlCl_3 + AlCl_4^- \rightarrow Al_2Cl_7^-$

$2\ AlCl_4^- \rightarrow Al_2Cl_7^- + Cl^-$

The electrochemical characterization of the reaction mechanisms that occur at the electrode-electrolyte interface, in the ionic liquids produced a wealth of information that was published in the scientific literature[24], [60] and [61]. From the data reported, we can understand which chemical phenomena occur during the process and how to set the parameters in order to obtain good results.

The aluminum electrodeposition process from ionic liquids takes place by three steps:

1. Weak coordinate bond breaking, between chloroaluminate specie and the organic cation.
2. Strong coordinate bond breaking in the aluminum complexes, in order to release aluminum cation Al^{3+}, by the reactions

$AlCl_4^- \rightarrow Al^{3+} + 4Cl^-$

$Al_2Cl_7^- \rightarrow 2Al^{3+} + 7Cl^-$

3. The process that allows aluminum reduction by gaining three electrons

$Al^{3+} + 3e^- \rightarrow Al$

The final reaction that takes place at electrode-electrolyte interface is:

$4Al_2Cl_7^- + 3e^- \rightarrow Al + 7AlCl_4^-$

The aluminum reduction process must involve a decrease of trivalent aluminum cation concentration in the electrochemical bath. In order to compensate this drop, an aluminum counterelectrode is used. So, the anodic discharge that occurs on the auxiliary electrode is:

$Al + 7AlCl_4^- \rightarrow 4Al_2Cl_7^- + 3e^-$

Several studies were focused on crystal nucleation and growth mechanisms. In the literature is reported that, in these conditions, the deposition occurs by instantaneous nucleation and following grain growth [60]. That means there some difficulties in the nucleation mechanism, and in fact analyzing the deposits by optical and scanning electron microscope it is possible to observe the surface structure, which shows grain size with order of μm.

ORIGINAL RESEARCH SECTION.

6 Deposition of nanocrystalline aluminum layers, by electrodeposition.

In the last few years, studies focused on the development of nanocrystalline materials have become a well established area of science. By definition, nanocrystalline materials are polycrystalline solids with a grain size smaller than 100 nanometers.

Nanocrystalline materials show peculiar properties due to their small grain size that increases the number of atoms located in the grain boundaries. In fact they show, compared to polycrystalline materials, increased strength/hardness, enhanced diffusivity, improved ductility/toughness, reduced elastic modulus, higher electrical resistivity, higher thermal expansion coefficient, lower thermal conductivity, and superior soft magnetic properties.

Nanocrystalline materials are usually classified into four different categories:

(a) nanocluster materials and nanodispersions (0D),
(b) layered or lamellar structures (1D),
(c) filamentary structures (2D),
(d) equiaxed nanostructured materials (3D).

Zero-dimensional nanomaterials include nanocluster materials and nanodispersions, i.e. materials in which nanoparticles, with a diameter less than 100nm, are isolated from each other.

A layered or lamellar structure is a one dimensional nanostructure in which the thickness is less than 100 nanometers in size, whereas the length and width are much greater.

The two-dimensional nanostructure, termed filamentary, it is a rod-shaped nanostructure; in this the length is larger than width or diameter, which are of nanometer dimensions.

The equiaxed nanostructured materials has all the three dimensions are of nanometer size and are also termed nanostructured crystallites [62].

Nanocoatings are usually classified as one-dimensional nanomaterials. They are particularly interesting because they significantly enhance the ability of a coating to improve surface properties. It's well-known that the strength of metallic materials can be drastically

increased by decreasing their grain size to the nanometer range, according to the Hall-Petch relationship [63].

Nanocrystalline coatings can be obtained by means of the addition of electroactive species into the electrochemical bath. Several studies have investigated the influence of organic additives in the plating bath [64], [65], [66], [67], [68] and [69]. Some additives showed interesting achievements regarding to the improvement of the morphology and physical properties of metal deposits, for example saccharin, thiourea and others compounds are commonly used as leveling and brightening agents in electroplating. In the following chapters, we will describe the approach used in the present study to develop such precursors for aluminum electrodeposition.

6.1 Experimental details.

6.1.1 Preparation of the solution and electrochemical bath.

Because of their high hygroscopic characteristics, ILs and other chemicals used in the present study were handled inside a glove box filled with dry nitrogen atmosphere. Before the preparation of the ionic liquid, 1-ethyl-3-methylimidazolium chloride (>99 %, Io-li-tec) was dried under vacuum condition at 60 °C for 20 h, to remove residual moisture. Anhydrous aluminum chloride (anhydrous powder, 99.99 %, Sigma Aldrich) was employed as received. The $AlCl_3$-[EMIm]Cl ionic liquid (1.5 : 1 molar ratio $AlCl_3$ to [EMIm]Cl, ensuring Lewis acidic ionic liquid) was prepared by slow addition of known weights of $AlCl_3$ to [EMIm]Cl in a beaker. A light white smoke was observed during preparation due to highly exothermic reaction occurring between $AlCl_3$ and [EMIm]Cl components, and care must to be taken to control the reaction rate and avoid the decomposition of the electrolytes. The experiments were conducted by adding 6 different organic compounds: acid glutaric, 1-methoxy naphthalene, 2-chloro nicotinic acid, poly(ethylene glycol) methyl ether, glycolic acid, 2-pyridine sulfonic acid. All the compounds were supplied by Aldrich, and used as received without further purification.

As liquid precursors 1-methoxy naphthalene and poly(ethylene glycol) methyl ether were used at a concentration of 5 ml l^{-1}, . Regarding solid precursors acid glutaric, 2-chloro nicotinic acid, glycolic acid and 2-pyridine sulfonic acid were used and dissolved at concentrations of about 4 g l^{-1}.

6.1.2 Electrochemical experiments.

Cyclic voltammetry experiments were carried out in the glove box using a three-electrode electrochemical cell and an Autolab PGstat20 Potential/Galvanostat. The counter electrode was an aluminum foil (99.99 %, Goodfellow) and the reference electrode was an Al-wire (99.99 %, Goodfellow) of 2 mm in diameter. Prior to use, the counter and reference electrodes were mechanically polished with increasingly finer grades of emery papers, cleaned with acetone and dried. As working electrode an iron foil, protected by zinc coating (Kiesow) was used. Before use, the working electrode was prepared. At the beginning, the zinc coating was removed by 1 M hydrochloric acid and then the iron substrate was polished by emery paper, cleaned with acetone and dried.

6.1.3 Electrodeposition and characterization of the aluminum coatings.

The 1.5:1 molar ratio $AlCl_3$-[EMIm]Cl ionic liquid was used for the electrodeposition of aluminum. Constant potential deposition of aluminum was performed on Fe electrodes in the three-electrode cell as describe in section 6.1.2. The size of the cathode and the anode was 0.5x0.5 cm, and the distance between them ca. 0.5 cm. Following each deposition experiment, the resulting of the deposition was thoroughly rinsed with water, acetone and dried cool air. The surface morphologies of the deposits were then examined by scanning electron microscope, while the chemical compositions were obtained by X-ray microanalysis

6.2 Results and discussion.

6.2.1 Cyclic voltammetry.

Before going into the investigation of the influence of organic additives on the system behavior, a study about how the temperatures affect it was carried out. The study compares the cyclic voltammogram recorded on the iron surface, in Lewis acidic ionic liquid [EMIm]Cl/$AlCl_3$ (1:1.5 molar ratio), at two different temperatures: at room temperature (25 °C) with black line and at 100 °C with red line.

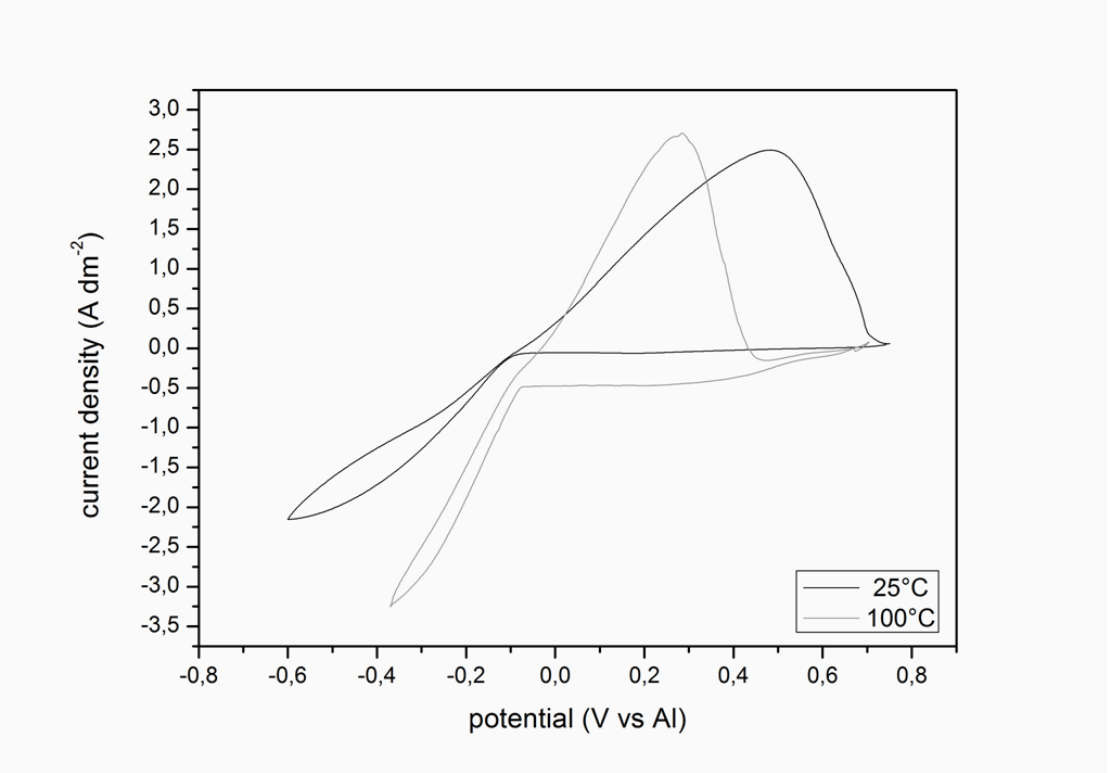

Figure 15 Cyclic voltammogram of Al deposition on iron surface in Lewis acidic ionic liquid [EMIm]Cl/$AlCl_3$ (1 : 1.5 molar ratio), at 25 °C (black line) and at 100 °C (red line), with scan rate of 10 mVs^{-1}.

The electrode potentials were scanned from the open circuit potential in the negative direction at rate of 10mV s^{-1}. As it can be seen, at room temperature, a rising cathodic current, corresponding to the bulk Al deposition, stars at around -100 mV. In the reverse scan a current loop is recorded, which indicates that bulk Al deposition on iron electrode is initiated by an overpotential driven nucleation process which is characteristic for many of its analogues in ionic liquids. Concerning the oxidation peak, attributed to the reversible stripping of Al, it is centered at about +500 mV, at room temperature.

In regard to the cyclic voltammogram recorded at 100 °C, can be seen that the bulk Al deposition stars at a less negative potential, at around -50 mV, as well as oxidation peak occurs at less positive potential, at about +300 mV. Furthermore, the peak current of deposition significantly increases as the temperature increases showing an increase of the reaction rate. For this reason, the cyclic voltammogram recorded at 100 °C was reversed at less negative potential. The increasing of the reaction rate, as well as the decreasing of the separation between the cathodic and anodic peaks, are attributed to the charge transfer and mobility of the electroactive species towards the electrode surface, with elevating temperature [70].

The electrochemical investigation, by cyclic voltammetry of Al deposition, on iron substrates and with a scan rate of 10mV s^{-1}, was conducted at 25 °C and 100 °C, adding the organic additives to the electroplating bath. In Figure 16, 17 and 18 were reported the series of cyclic voltammograms obtained at 25 °C and in Figure 19, 20 and 21 the series of cyclic voltammograms obtained at 100 °C. Every graph compares the voltammogram recorded adding one organic compound to the electrochemical bath (red line) and using the pure ionic liquid as electrolyte (black line), at the same temperature.

6.2.2 Organic additives.

The aim of this approach is to investigate the influence of organic additives on aluminum electrodeposition, in particular on the crystallite sizes of the Al film:

a) Glutaric acid
b) 1-methoxy naphthalene
c) 2-chloro nicotinic acid
d) poly(ethylene glycol) methyl ether
e) glycolic acid
f) 2-pyridine sulfonic acid

In order to study the system behaviour cyclic voltammetry was carried out. Recorded cyclic voltammograms using the pure ionic liquid and with the addition of one of the six organic compounds were compared. Moreover the investigation also analyzed the influence of temperature on the process, so the experiments were carried out at two different temperatures: 25 °C and 100 °C. Regarding the characteristics of obtained aluminum deposits, constant potential depositions were performed and also in this case experiments were carried out at two different temperatures.

Comparing the voltammograms obtained in these conditions, it is possible to observe common tendencies (there are just two exception: for the glutaric acid at 25 °C and for the glycolic acid at 100 °C). As can be seen, in presence of the additives the bulk Al deposition stars at more negative potential, compared to the pure ionic liquid. This phenomenon can be connected to the adsorption of the additives on the substrate surface. In fact when the overpotential increases, the nucleation activation energy and the density of nucleating grain precursors increases and the result is a decrease of the grain size [71].

2 - CHLORONICOTINIC ACID

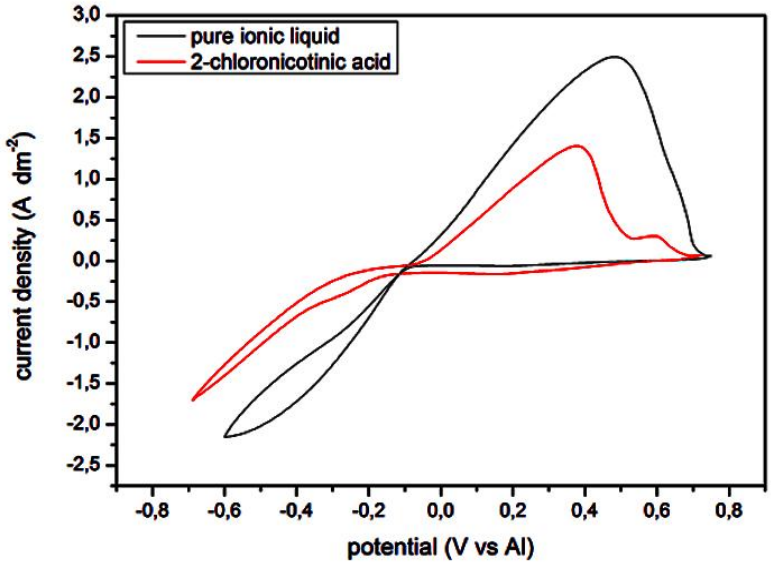

GLYCOLIC ACID

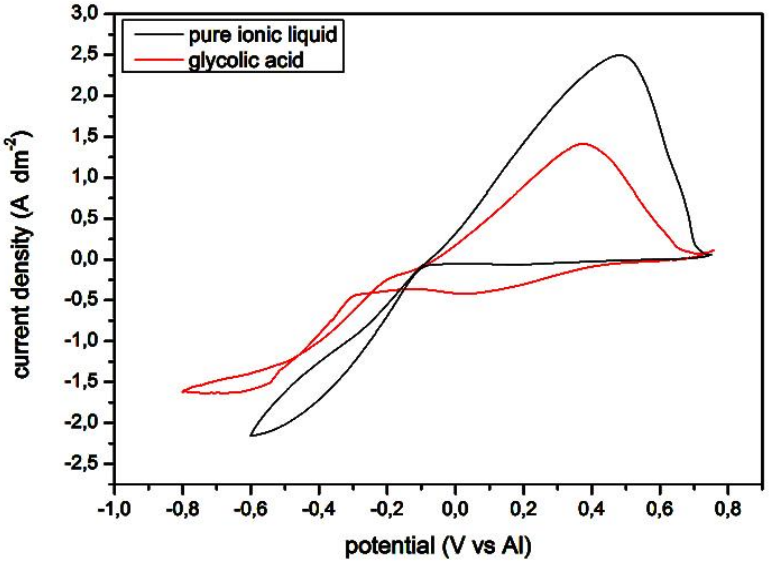

Figure 16 Graphs comparing the cyclic voltammogram of Al deposition, on an iron surface at 25 °C and with scan rate of 10 mVs^{-1}, in pure ionic liquid [EMIm]Cl/$AlCl_3$ (40 % / 60 %) (black line) and with the cyclic voltammogram obtained adding 2-chloronicotinic acid and glycolic acid to the pure ionic liquid (red line).

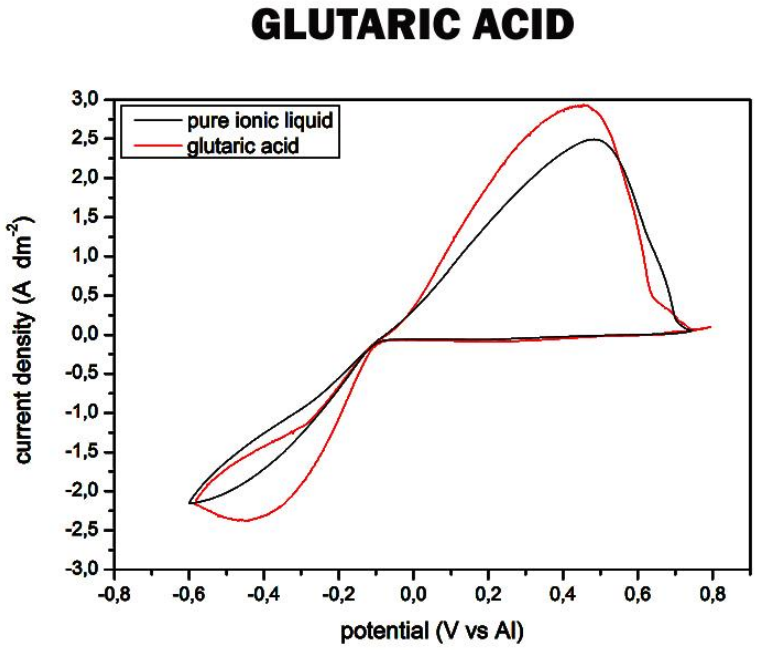

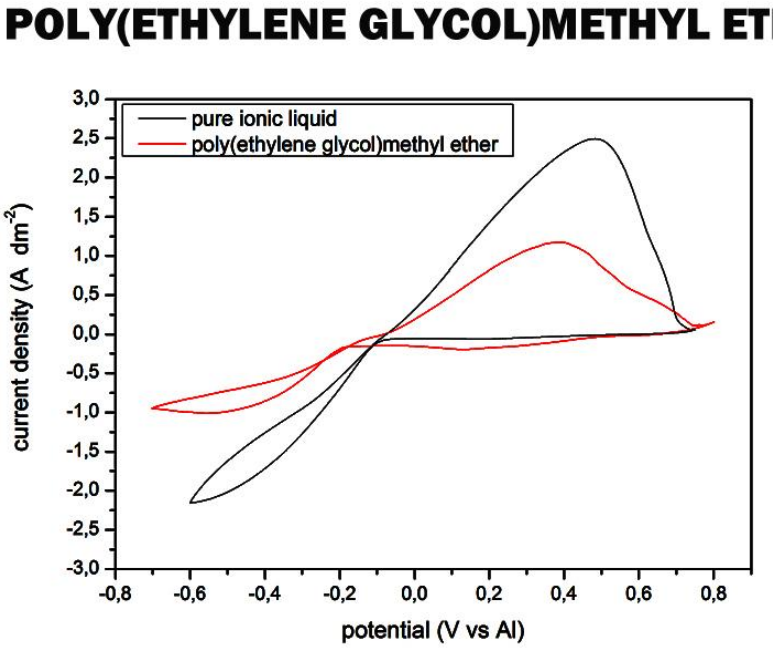

Figure 17 Graphs comparing the cyclic voltammogram of Al deposition, on an iron surface at 25 °C and with scan rate of 10 mVs^{-1}, in pure ionic liquid [EMIm]Cl/$AlCl_3$ (40 % / 60 %) (black line) and with the cyclic voltammogram obtained adding glutaric acid and poly(ethylene glycol)methyl ether to the pure ionic liquid (red line).

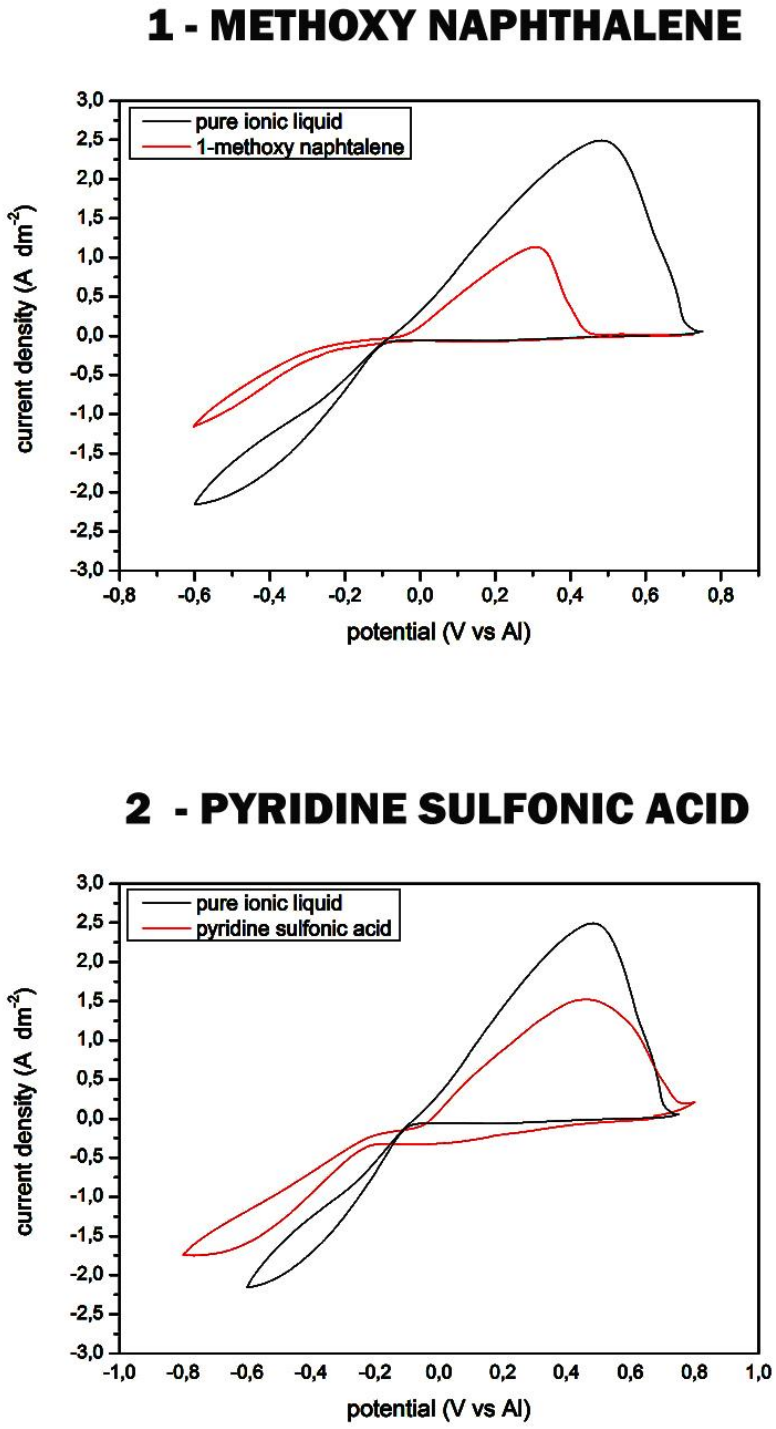

Figure 18 Graphs comparing the cyclic voltammogram of Al deposition, on an iron surface at 25 °C and with scan rate of 10 mVs^{-1}, in pure ionic liquid [EMIm]Cl/$AlCl_3$ (40 % / 60 %) (black line) and with the cyclic voltammogram obtained adding 1-methoxy naphthalene and 2-pyridine sulfonic acid to the pure ionic liquid (red line).

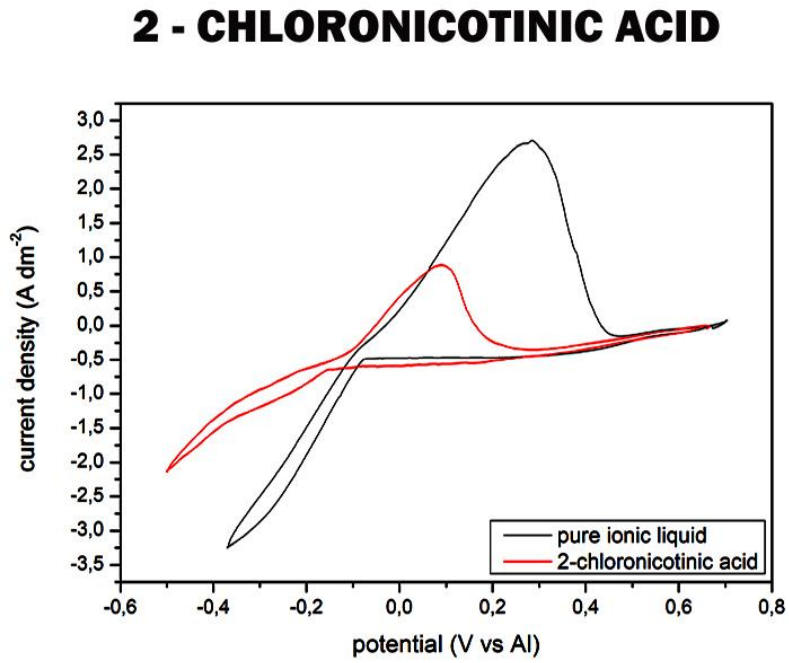

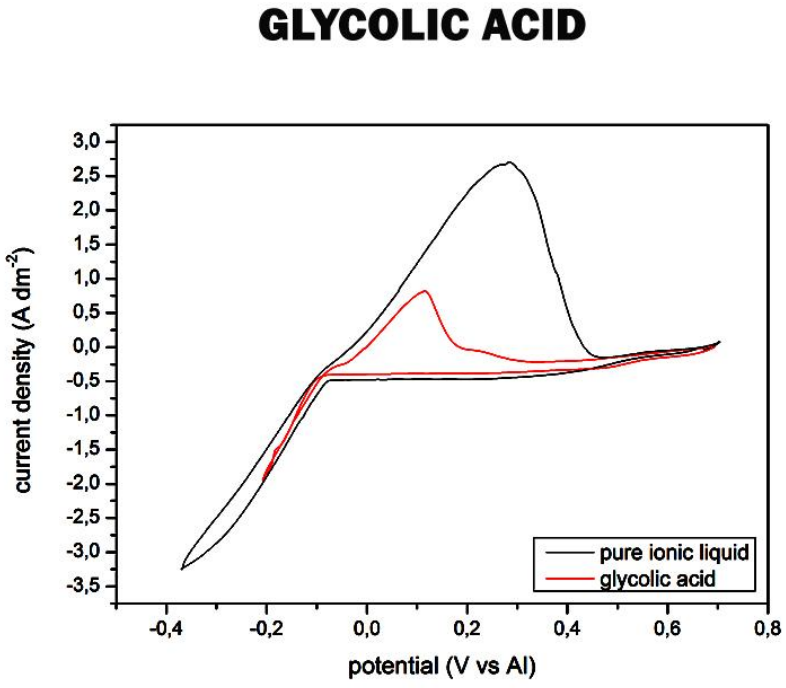

Figure 19 Graphs comparing the cyclic voltammogram of Al deposition, on an iron surface at 100 °C and with scan rate of 10 mVs^{-1}, in pure ionic liquid [EMIm]Cl/$AlCl_3$ (40 % / 60 %) (black line) and with the cyclic voltammogram obtained adding 2-chloronicotinic acid and glycolic acid to the pure ionic liquid (red line).

GLUTARIC ACID

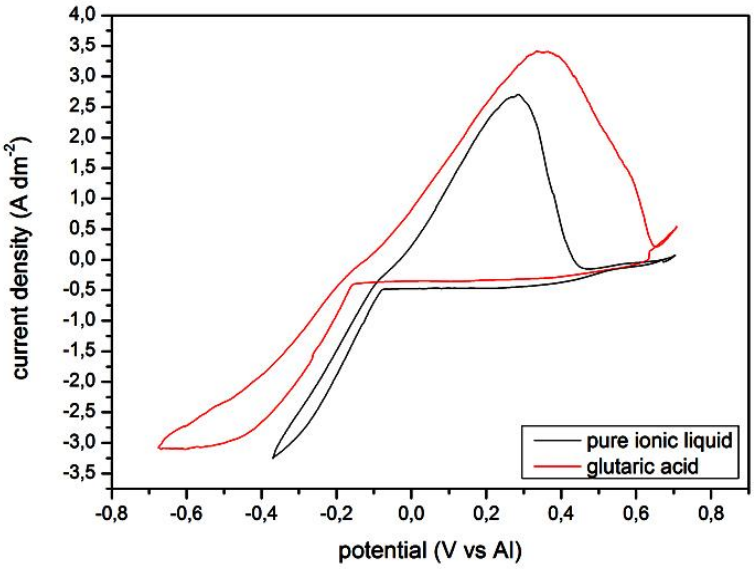

POLY(ETHYLENE GLYCOL)METHYL ETHER

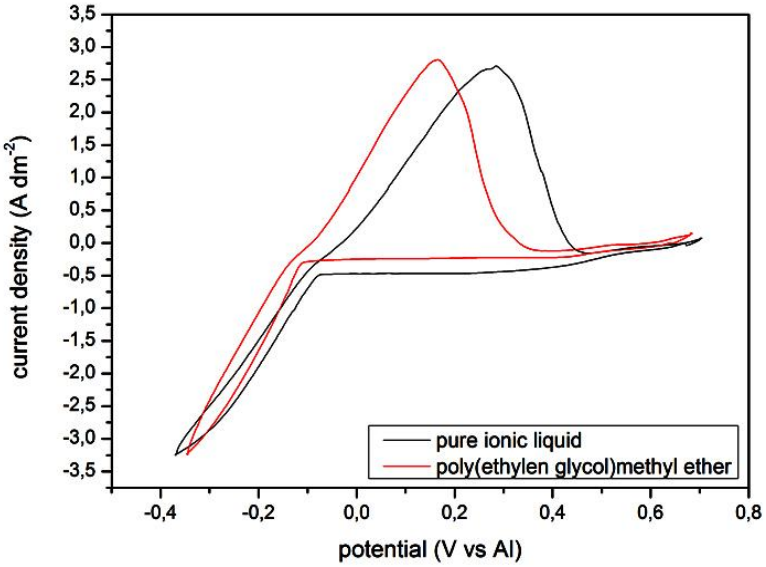

Figure 20 Graphs comparing the cyclic voltammogram of Al deposition, on an iron surface at 100 °C and with scan rate of 10 mVs^{-1}, in pure ionic liquid [EMIm]Cl/$AlCl_3$ (40 % / 60 %) (black line) and with the cyclic voltammogram obtained adding glutaric acid and poly(ethylene glycol)methyl ether to the pure ionic liquid (red line).

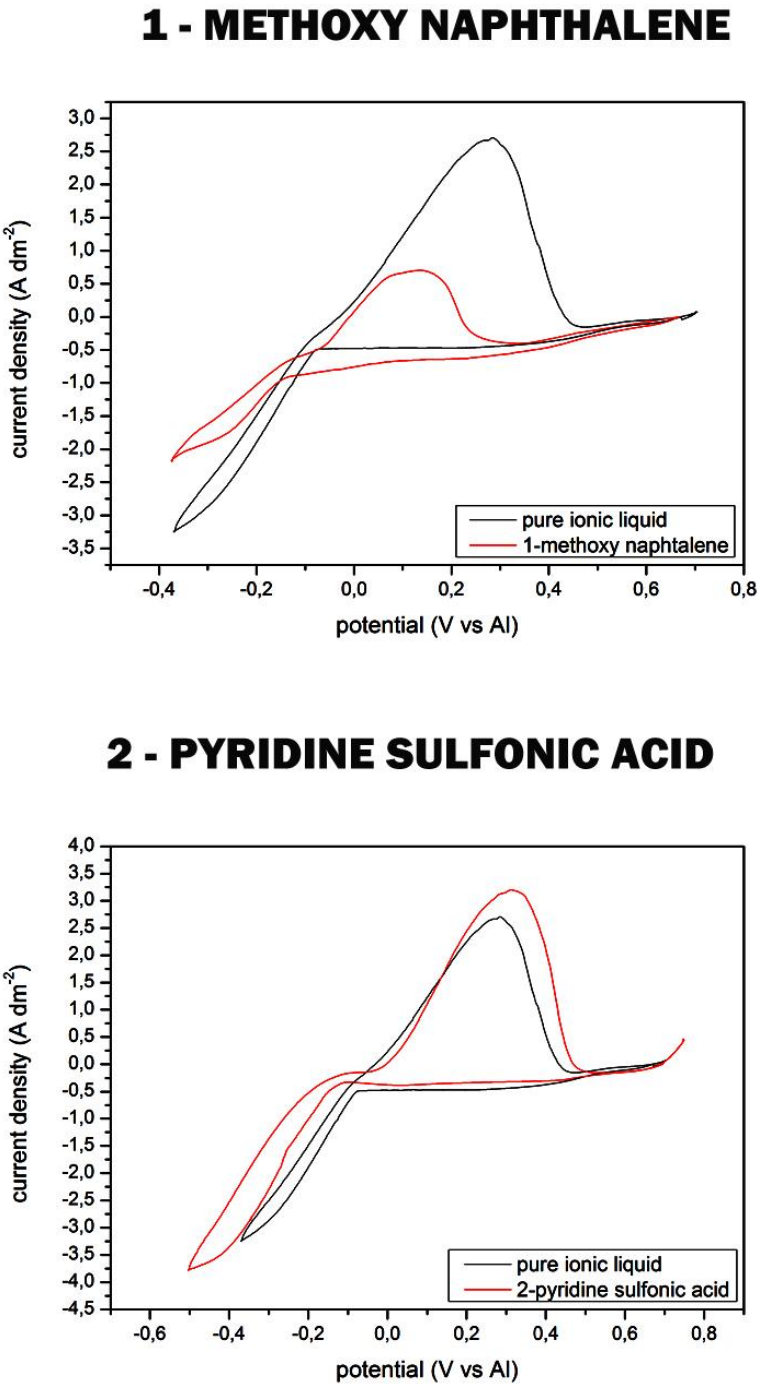

Figure 21 Graphs comparing the cyclic voltammogram of Al deposition, on an iron surface at 100 °C and with scan rate of 10 mVs^{-1}, in pure ionic liquid [EMIm]Cl/$AlCl_3$ (40 % / 60 %) (black line) and with the cyclic voltammogram obtained adding 1-methoxy naphthalene and 2-pyridine sulfonic acid to the pure ionic liquid (red line).

Two series of electrodepositions were carried out at constant potential in [EMIm]Cl/$AlCl_3$ with the addition of the different additives. One series at room temperature and the other one at 100 °C. In figure 16, 17 and 18 it is possible to observe the current loops attributed to the nucleation of aluminum and they can be taken as an indication of potentiostatic electrodeposition. At 25 °C, the electrodepositions were carried out on a potentiostatic way, E=-500 mV, for 1 hour. Visually, all the obtained Al layers show a bright and shiny surface that usually suggests an indication of the small crystal grain size. Adding 2-chloro nicotinic acid and 1-methoxy naphthalene, the coatings, in addition to the bright and shiny characteristics, have a particular "goldish" color.

The obtained bulk Al electrodeposits were investigated with a high resolution scanning electron microscope. Figure 22 shows the high resolution SEM micrographs of the aluminum deposits created at 25 °C. The pictures show that the obtained coatings are uniform with fine crystallites in the nanometer regime. This behavior can be explained by the use of organic additives which interact with the active growth sites by adsorption and thus act as grain refiners. The freshly deposited adatoms are forced to form new nuclei, resulting in the formation of a nanostructure.

Electrodepositions at 100 °C were carried out potentiostatically, but using lower constant potentials. The cyclic voltammograms obtained at 100 °C (Figure 19, 20 and 21) show quite different potentials of Al deposition depending on the different additive added to the ionic liquid. For this reason the electrodepositions were conducted at a potential E=-300 mV, for 1 hour. Not all the tests carried out at 100 °C showed good results. In fact, just by visual examination it has been possible to identify the coatings composed by fine grain size, that showed a bright and smooth surface.

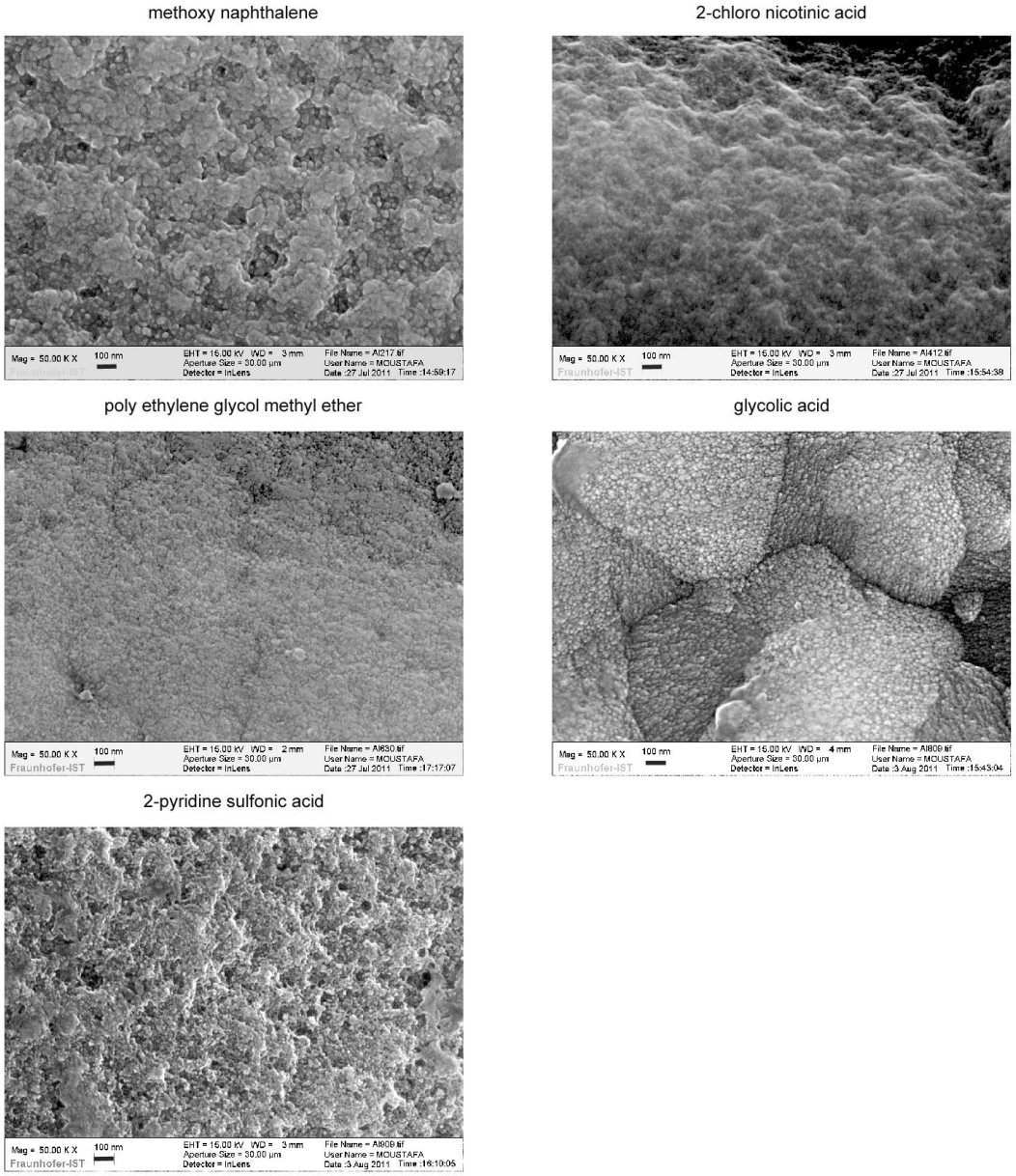

Figure 22 SEM micrographs of electrodeposited Al on iron in [EMIm]Cl/$AlCl_3$ (1:1.5 molar ratio) and the different organic compounds (1-methoxy naphthalene, 2-chloro nicotinic acid, poly(ethylene glycol) methyl ether, glycolic acid and 2-pyridine sulfonic acid). The deposits were obtained after potentiostatic polarization for 1 h at a potential of -500 mV, at 25 °C.

They are the coatings obtained by the addition of 1-methoxy naphthalene and 2-chloro nicotinic acid to the electroplating bath. The coatings obtained by the addition of 2-chloro nicotinic acid, presents the same goldish shining surface, as that one realized at 25 °C. For this reason, SEM analyses were limited to these two samples. The micrographs are reported in the figure below.

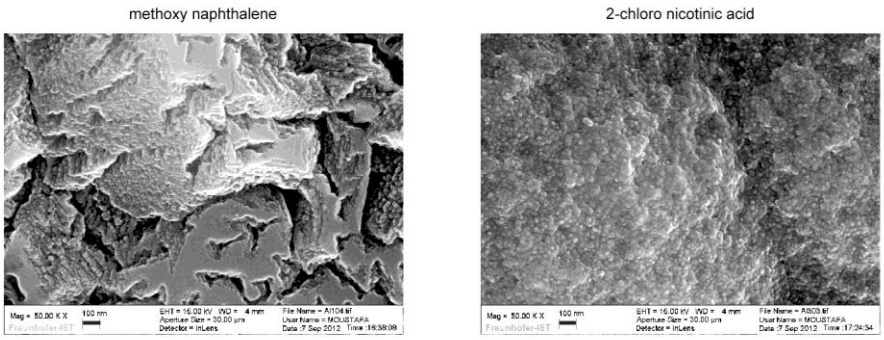

Figure 23 SEM micrographs of electrodeposited Al on iron in [EMIm]Cl/$AlCl_3$ (1:1.5 molar ratio) adding 1-methoxy naphthalene and 2-chloro nicotinic acid. The deposits were obtained after potentiostatic polarization for 1 h at 100 °C at a potential of -300 mV.

The coatings obtained are uniform and smooth. By addition of 1-methoxy naphthalene and 2-chloro nicotinic acid to the electroplating bath, the deposits obtained are composed by nanocrystalline aluminum.

6.2.3 Experiments outside the glove box.

In this section I describe a new technique to perform aluminum electrodeposition outside the glove box which normally provides the dry and oxygen free conditions necessary for maintaining intact the composition of the electrolyte. In this series of experiments, instead, in order to protect the electrochemical bath from the atmospheric moisture, an inert gas (Argon) was pumped by a nozzle submerged in the ionic liquid. In such a way it was possible to obtain an Argon layer over the bath, so that it isolated the bath from the moisture presents in the air.

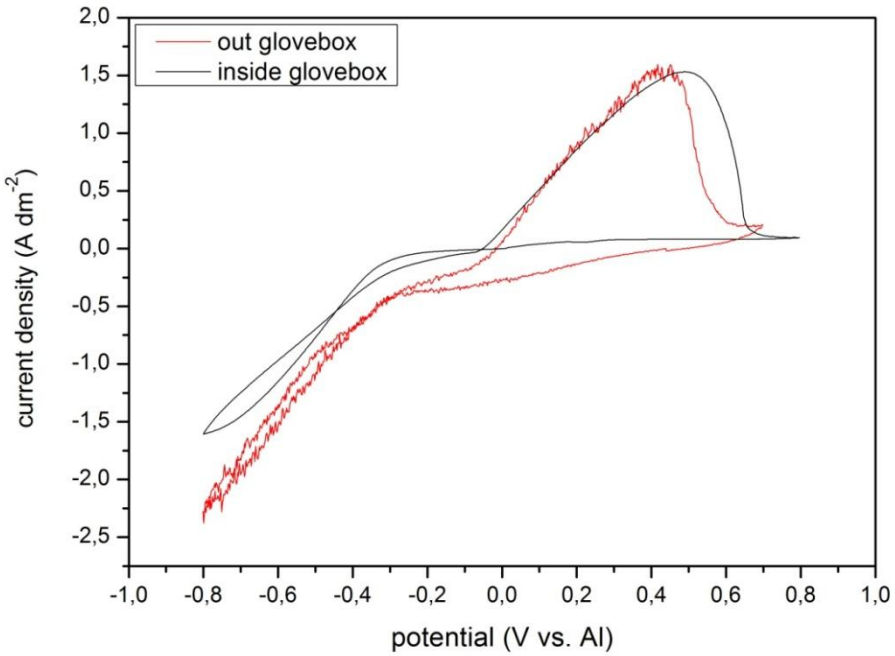

Figure 24 Cyclic voltammograms of Al deposition on iron surface in Lewis acidic ionic liquid [EMIm]Cl/$AlCl_3$ (1:1.5 molar ratio), adding 2-chloronicotinic acid, with scan rate of 10 mVs^{-1}, at 25 °C inside glove box (black line) and out glove box (red line).

To test this new approach, aluminum electrodeposition was performed adding to the electrochemical bath the organic compound who showed the best result, i.e. 2-chloronicotinic acid. As can be seen in the figure below, the cyclic voltammetry results do not show important differences in comparison with the ones one obtained inside the glove box.

Outside the glove box, the bulk Al deposition starts at potential slightly more negative, while the oxidation peak occurs at potential slightly less positive compared to the curve obtained inside the glove box.

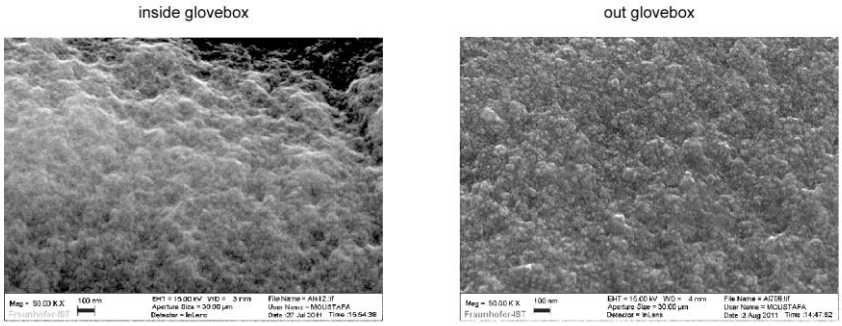

Figure 25 SEM micrographs of electrodeposited Al on iron in [EMIm]Cl/$AlCl_3$ (1:1.5 molar ratio) adding 2-chloro nicotinic acid, inside and out glove box. The deposits were obtained after potentiostatic polarization for 1 h at 25 °C, at a potential of -500 mV inside the glove box and at a potential of -600 mV out glove box.

The curve obtained out glove box appears noisier than the other one, but it can be easily attributed to flushing the bath with the inert gas. Outside of the glove box, the electrodeposition was obtained in potentiostatic mode, setting a constant potential E=-600 mV for 1 hour. Visually, the Al layer obtained out glove box has a gold-like shining surface similar to the one obtained inside the glove box. The high resolution SEM micrographs of the two cases are shown below. Again, the differences are minor and the deposit is uniform with a very fine crystallites in the nanometer range. This set of experiments show the importance of precursors to control the texture of aluminum layers electrodeposited in ionic liquid solutions and the possibility of performing the deposition in conditions that are promising for future industrial applications.

7 Aluminum-silicon coatings.

The main target of this approach aims at finding a new method to produce a strong coating that could have application as a protective layer for industrial gas turbines hot parts, operating in extreme conditions. Such turbine parts undergo mainly three kinds of stress: thermo-mechanical stress, hot corrosion phenomena and high temperature oxidation. To resist he thermo-mechanical stress, these turbine components are manufactured using nickel-based or cobalt-based superalloys, thus, they achieve an excellent creep resistance, even at high temperatures (T °C > 1000 °C). Unfortunately, such alloys do not have a good resistance to oxidation and to hot corrosion for the complete range of working temperatures.

Hot corrosion can be defined as accelerated corrosion, resulting from the presence of salt contaminants such as molten salts of the alkali metals (mainly sulphates), that combine to form molten deposits, which damage component's surface [72]. In Figure 26 it is possible to observe hot corrosion effects on a turbine blade surface [73].

Figure 26 Hot corrosion effects on turbine blade surface [73].

Hot corrosion is divided into two forms of attack: Type I (or high-temperature hot corrosion) and Type II (or low-temperature hot corrosion). They show different mechanism of attack, corrosion morphology and operating temperature range.

✓ Hot corrosion Type I (HTHC).

This form of hot corrosion occurs mainly within the temperature range 850 ± 950 °C. The process starts with the condensation of fused alkali metal salts on the surface of the component. Because of that, a series of chemical reactions take place, initially attacking the protective oxide layer and then starting to consume the substrate material. The dominant salt in HTHC is Na_2SO_4 due to its high thermodynamic stability. Sodium mainly derives from marine atmosphere (sea salts contain Na_2SO_4 and NaCl), but it can also come from industrial atmospheric pollutants and in the fuel. Moreover, in the fuel is also present sulfur, so during combustion, sodium sulfate can form from sodium and sulfur. Other impurities are present both in the fuel and or in the air, such as vanadium, phosphorus, lead and chlorides. They can combine with sodium sulfate to form a mixture of salts with a lower melting temperature, in this way the range of attack becomes wider. HTHC can generally be divided into four progressive stages:

a) In the first stage the surface becomes rougher, due to some growth and localized breakdown of the oxide scale layer. At this stage, neither consumption of the substrate layer nor loss of mechanical integrity are observed.

b) In the second stage the roughness of the surface is more marked because oxide layer breakdown continues. At this stage even a consumption of the substrate begins, as mechanical integrity is still not affected.

c) In the third stage oxidation of the substrate material has penetrated to significant depth. At this stage, even mechanical integrity is affected. Progression to fourth stage will go on with or without the presence of sodium.

d) In the fourth stage the attack penetrates deeply into the bulk. Corrosion process is so advanced that it causes the loss of structural material [72].

Microscopically, HTHC is characterized in many cases by severe peeling of the metal and by significant color changes. The Type I hot corrosion morphology is typically characterized by a thick, porous layer of oxides with the underlying alloy matrix depleted in chromium. The reaction products frequently exhibit oxide precipitates dispersed in the salt film [74].

✓ Hot corrosion Type II (LTHC).

This form of hot corrosion is observed mainly within the temperature range 650 ± 800 °C. In particular, the corrosion rate due to the salts reaches a maximum around 750 °C for Ni- and Co- based alloys. The Type II hot corrosion is characterized by pitting morphology with little or no internal penetration of the corrosion under the pit. It results from the formation of mixtures of Na_2SO_4 and $CoSO_4$ with low melting temperatures. For example $CoSO_4$ is a corrosion product of a reaction between the surfaces made of Co-based alloy and SO_3 from the combustion gas. The formation of $NiSO_4$-Na_2SO_4 eutectics occurs in a similar way for Ni-based superalloys. Chloride contained in the exhaust gases attacks locally the surface and causes localized failure of the scale, as well as thermal cycling and erosion. In these spots LTHC begins as localized pitting. As opposed to Type I hot corrosion, in Type II neither incubation period nor microscopic sulfidation and chromium depletion are observed [72].

Regarding high temperature oxidation, in principle the superalloys are oxidation resistant but, when oxygen is present, all the metals will be slowly oxidized. The oxidation rate depends on different factors: alloy composition, oxygen concentration, temperature, etc. Unfortunately, alloys designed for maximum strength do not show a high resistance against oxidation [75].

In general, surface oxidation involves the formation of a relatively uniform thick oxide layer. In some cases, a light and uniform surface oxidation can be useful to prevent a deeper corrosion. However, intergranular oxidation can create serious problems and it can reduce fatigue resistance. Superalloys, and in particular nickel-based alloys, are subject to intergranular oxide penetration. Moreover, the advancing of oxide front is preceded by alloy change in composition generated by depletion of the most easily oxidized component, typically aluminum. The depleted zone is weaker than the normal alloy and it affects the strength properties of the alloy. Even the stress has an effect on the rate of oxidation. The data indicate that oxidation proceeds at constant rate with increasing stress up to a critical point. Afterward, oxidation proceeds faster and in some cases catastrophically. In general, the oxidation resistance of simple nickel- and cobalt-based alloys is considered to be relatively good as the oxides formed are firmly adherent and protective up to about 800 °C.

Above this temperature, oxidation becomes a problem, especially for more complex superalloys as the addition of the elements that give the alloys elevated-temperature strength (i.e. titanium and molybdenum) decreases the oxidation resistance [75].

Some papers showed that higher concentration of chromium in the alloy promotes the development of Cr_2O_3, that is more effective than, for example, Al_2O_3 in particularly against Type II corrosion because it is more stable compared molten salts, [42],[43],[76] and [77]. In particularly, regarding chromium and aluminum coatings, there is a military specification (MIL-DTL-5541) that concerns chromate conversion coatings for aluminum and aluminum alloys and describes their properties and purposes. Chromium or Al-Cr and Al-Cr-Pt diffusive treatments (among which pack and CVD processes) are decribed in [78], [79], [80], [81], [82] and [83]. The state-of-art procedure to optimize engine efficiency is constituted of two possibilities:

1) MCrAlY coatings (where M = Ni, Co or Ni/Co) obtained by thermal spray process [84], [85], [86] and [87]
2) Diffusion coatings based on the intermetallic compound Ni-Cr, obtained by chromizing treatments on superalloys [88] and [89]

Chromatization is the cheapest process to obtain suitable Cr coatings, but it is a problematic process from an environmental viewpoint because of the presence of chromium (VI) in the waste products and gradually national and international legislation restricts the use of this extremely toxic compounds.

Our approach in the present study considers the possibility to replace the chromatization process with Al-Si composite coatings. It is already known that increasing the superficial concentration of Al and Si can improve the corrosion resistance of superalloys, in particularly against hot corrosion Type II [90] [91] [92] [93] and [94]. Hence, an intermetallic compound of aluminum and silicon as coating is expected to provide good results to protect the substrate against corrosion; in particular, such a layer could provide:

- ✓ Protection for a wider range of temperature (not just against hot corrosion type II, but even against hot corrosion type I and high temperature oxidation).

✓ Protection for the same or even longer time.

Hence, the aim of the present project was to obtain Al-Si alloys by electrodepositon, from $AlCl_3$-[BMIm]Cl ionic liquid, of an aluminum composite containing dispersed Si metallic particles.

In order to control the concentration and distribution of silicon particles in the coating, a systematic study of three parameters was conducted: concentration and grain size of silicon particles in the electrochemical bath and stirring speed for homogenizing the suspension. Moreover the electrodeposition, carried out by galvanostatic mode, was executed using a different current/time function profile.

7.1 Experimental details.

The ionic liquid 1-butyl-3-methylimidazolium chloride / aluminum chloride in molar ratio 1:2 was supplied by Aldrich, and used as received. Two different grain sizes of silicon metallic particles were testes (both supplied by Aldrich):

- Mesh -100 ÷ +200 (75 µm ≤ Ø ≤ 152 µm)
- Mesh -325 (Ø ≤ 60 µm)

The experiments were conducted using three different concentrations of silicon particles in the electrochemical bath:

- [Si] = 0.5 g/l
- [Si] = 1.0 g/l
- [Si] = 2.0 g/l

The experiments were conducted inside a glove box, and the galvanostatic depositions were performed using a potentiostat/galvanostat Parstat 2273. The surface morphology of the deposits was then examined by scanning electron microscope, while the chemical compositions were obtained by X-ray microanalysis.

7.1.1 Electrochemical experiments.

Electrodeposition experiments were carried inside the glove box, using an electrolytic cell and an Autolab PGstat20 Potential/Galvanostat. The counter electrode was an aluminum foil (99,99 %, Goodfellow) and as working electrode was employed an copper foil (99 % Goodfellow). Prior to use, the counter and working electrodes were mechanically polished with increasingly finer grades of emery papers, cleaned with acetone and dried.

Because silicon distribution in the aluminum matrix is supposed to be directly linked to silicon distribution in the electrochemical bath, in order to obtain a homogeneous suspension the electrochemical bath was stirred by magnetic stirrer and six different stirring speeds were tested (50 rpm, 180 rpm, 310 rpm, 440 rpm, 570 rpm, 700 rpm). Electrodepositions were executed under galvanostatic control, using the normal constant current process and a pulse current function by an on/off profile.

In Figure 27 schematically shows the normal constant current profile, whereas the Figure 28 schematically shows the pulse current function by an on/off profile galvanostatic control. In this case a pulse current function applied a current value j_{pulse} during the time t_{on} and a current value equal to zero during the time t_{off}. The cycle t_{on}/t_{off} is repeated during the entire electrodeposition.

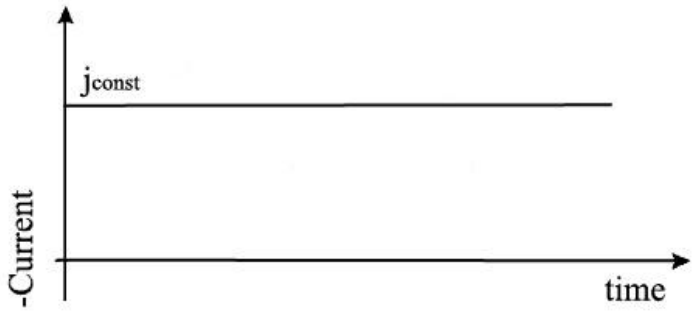

Figure 27 Constant current electrodeposition process, where j_{const} is the applied current during the deposition.

The experiments were carried out setting different values for the 3 parameters:

t_{on} was set equal to 3 seconds, 13 seconds, and 60 seconds;

t_{off} was set equal to 7 seconds, 17 seconds and 50 seconds;

j_{pulse} was set equal to -0.70 A/dm^2, -0.85 A/dm^2 and -1.00 A/dm^2.

The current pulsing technique was employed to obtain a homogeneous suspension. In fact, during the time t_{off}, when the electrodeposition is stopped, we can supposed that the homogeneous distribution of silicon particles in the electrochemical bath is re-established as it was at the beginning of the process.

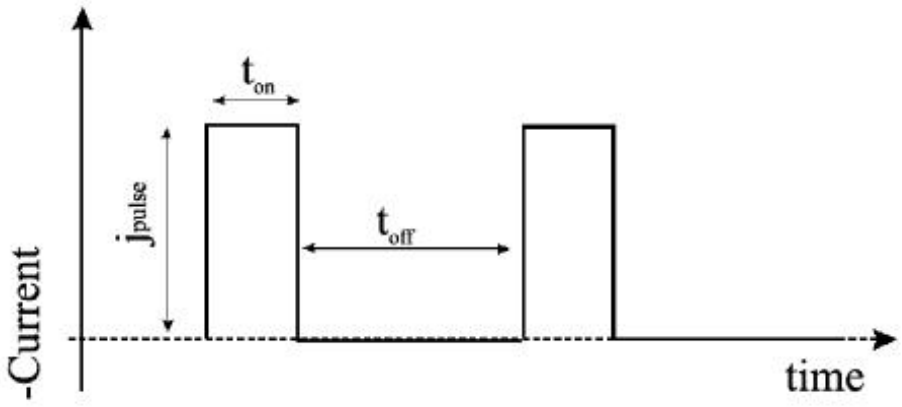

Figure 28 The pulse current function by an on/off profile. t_{on} is the time when the current j_{pulse} is applied and t_{off} is the time when the current is zero.

Pulse current, during the electrodeposition, can affect the diffusion layer next to the working electrode surface which is in contact with the liquid solution. This influences the deposition mechanisms of metal deposits and it can alter the nucleation process and the consequent growth of the deposit. By a pulsed current it is possible to incorporate nanoparticles to a high content in the coating as well as producing a wider range of alloys, deposit composition and material properties.

7.2 Results and discussion.

7.2.1 Current pulsing technique.

Errore. L'origine riferimento non è stata trovata., shows the results of using a pulse current function by an on/off profile during the electrodeposition. Pulsed electrodeposition prevents the manifestation of diffusion phenomena in the electrochemical bath. During the t_{off}, when the deposition is paused, the stirring removes the high concentration of reduction products close to the electrode and replaces them by fresh reactants, which reach the interface from the bulk solution. Consequently, every t_{off} step makes it possible to obtain a uniform distribution of the concentration of reagents. For this reason the potential recorded during

pulse current deposition is lower than the constant one that is driven by diffusion phenomena.

Deposits obtained using the two different galvanostatic techniques showed the same percentage of silicon. However, the aluminum layers obtained by pulse current deposition are visually smoother and bright, because this technique influences the mechanism of nucleation and growth of the deposit. We also found that stirring speeds have a significant role on the homogenization of the suspension. Electrodepositions were performed setting the stirring to six different speeds:

- 50 rpm (revolutions per minute)
- 180 rpm
- 310 rpm
- 440 rpm
- 570 rpm
- 700 rpm

Low speeds, as 50 rpm and 180 rpm, were not sufficient to keep silicon particles in suspension and they remained on the bottom of the beaker. Instead, speeds higher than 440 rpm determined the formation of a whirlpool in center of beaker, the electrodes were located. The result was to disrupt the normal aluminum deposition.

Applying a speed equal to 310 rpm, the stirring is enough to get silicon particles in suspension, but not so strong to interfere too much with the electrodeposition process.

In these conditions it was possible to obtain deposits including a good percentage of silicon

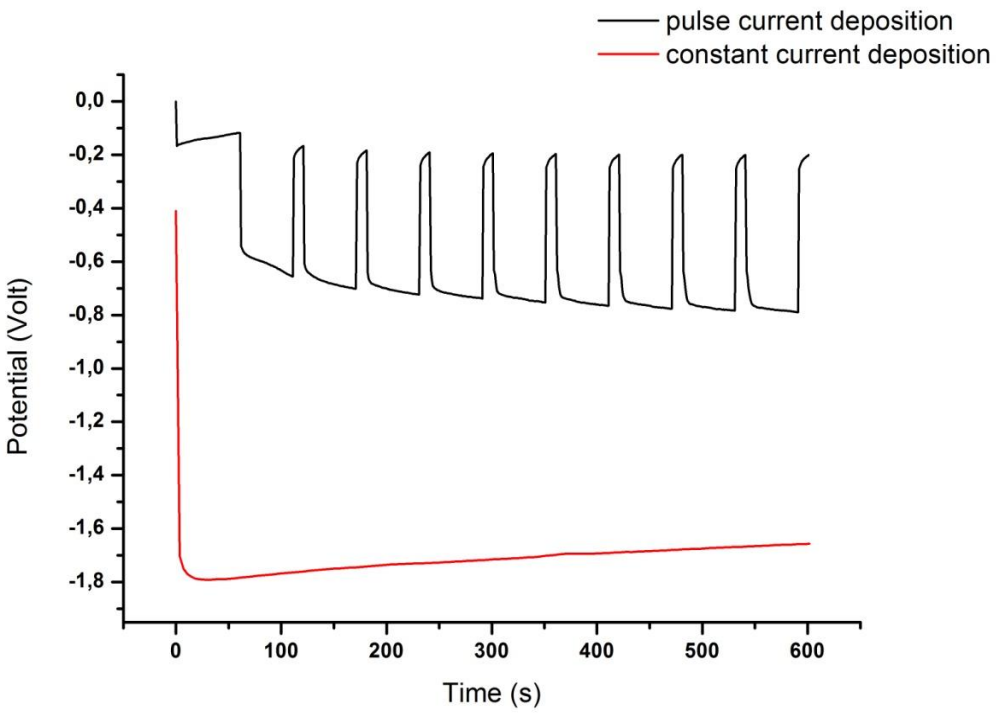

Figure 29 The graph compares the potential recorded during the electrodeposition by constant current function (red line) and by pulsed current function. The electrodeposition was conducted setting the same current density, j_{app} and j_{on} equal to 0.5 A dm^{-2} and the pulse current deposition parameters were: t_{on}= 50 s and t_{off} = 10 s.

particles, depending on parameters such as concentration and grain size of the silicon particles.

Regarding the grain size of silicon particles, the study started with adding to the electrochemical bath particles of size equal to -100 ÷ +200 mesh, that corresponds to diameter between 75 µm and 152 µm. In this case, the silicon concentration detected in the aluminum layers was very low, about 1 % and sometimes lower than the EDX detection limit. The main problem was probably related to the different grain size of silicon particles compared to that of aluminum crystals obtained by electroreduction, which are too small to include silicon. So, particles with a smaller mesh were tested. A mesh equal to -325,

corresponds to diameter smaller than 44 μm. In this case silicon metallic particles were smaller than the reduced aluminum grains deposited on the surface and they were included in the coating. In the figure below (fig 30), it is possible to observe a SEM micrograph of a silicon particle embedded in the aluminum layer. The EDX analysis shows aluminum crystals (red area) and the silicon particle (green area).

The silicon concentration was found to play a fundamental role in obtaining Al-Si coatings. The experiments were conducted testing three different concentrations of silicon particles in the electrochemical bath:

- [Si] = 0.5 g/l
- [Si] = 1.0 g/l
- [Si] = 2.0 g/l

The deposits obtained with a concentration of 0.5 g/l did not result in a detectable silicon concentration in the aluminum layer. Coatings showing detectable silicon were obtained using a concentration equal to 1.0 g/l and 2.0 g/l of silicon particles in the bath. In particular, the latter allowed obtaining an aluminum layer including about 7 % of uniformly distributed particles on the sample surface, as shown in Figure 33. In Figure 34 we show the EDX data about aluminum and silicon percentage detected in layer.

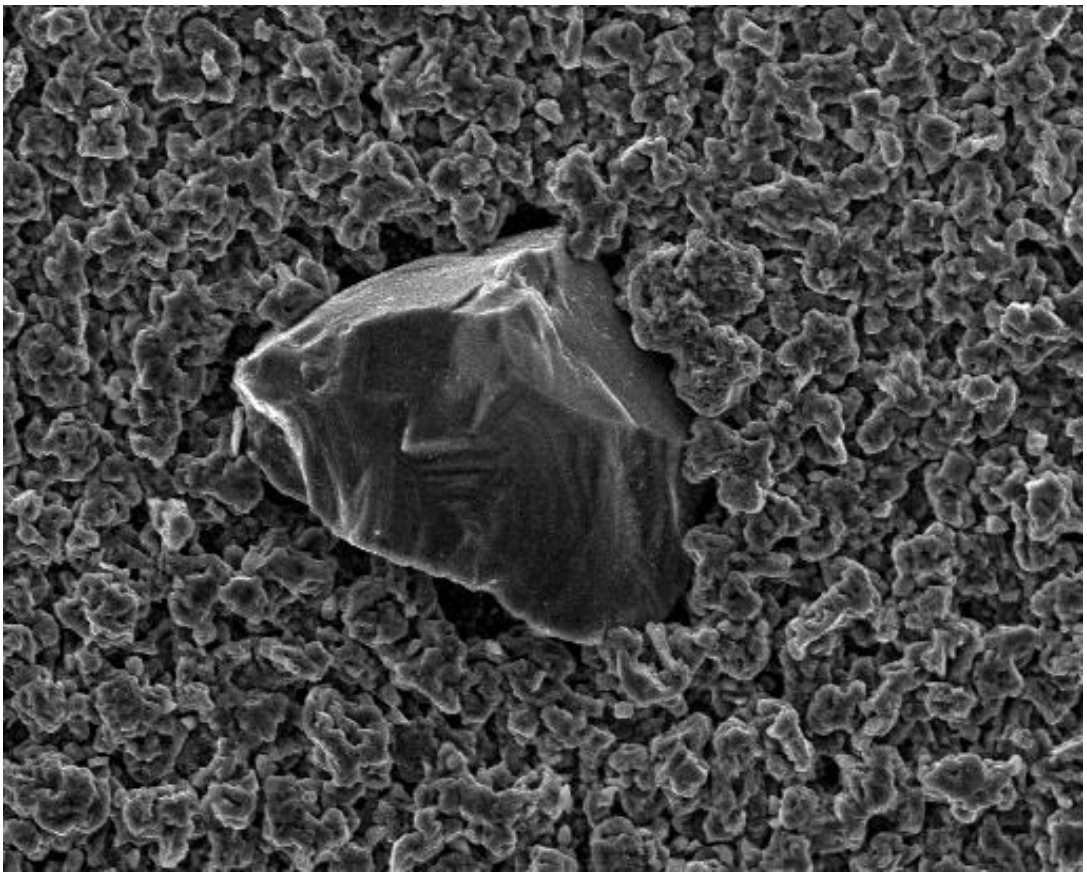

Figure 30 SEM micrograph of a silicon particle included in the aluminum layer.

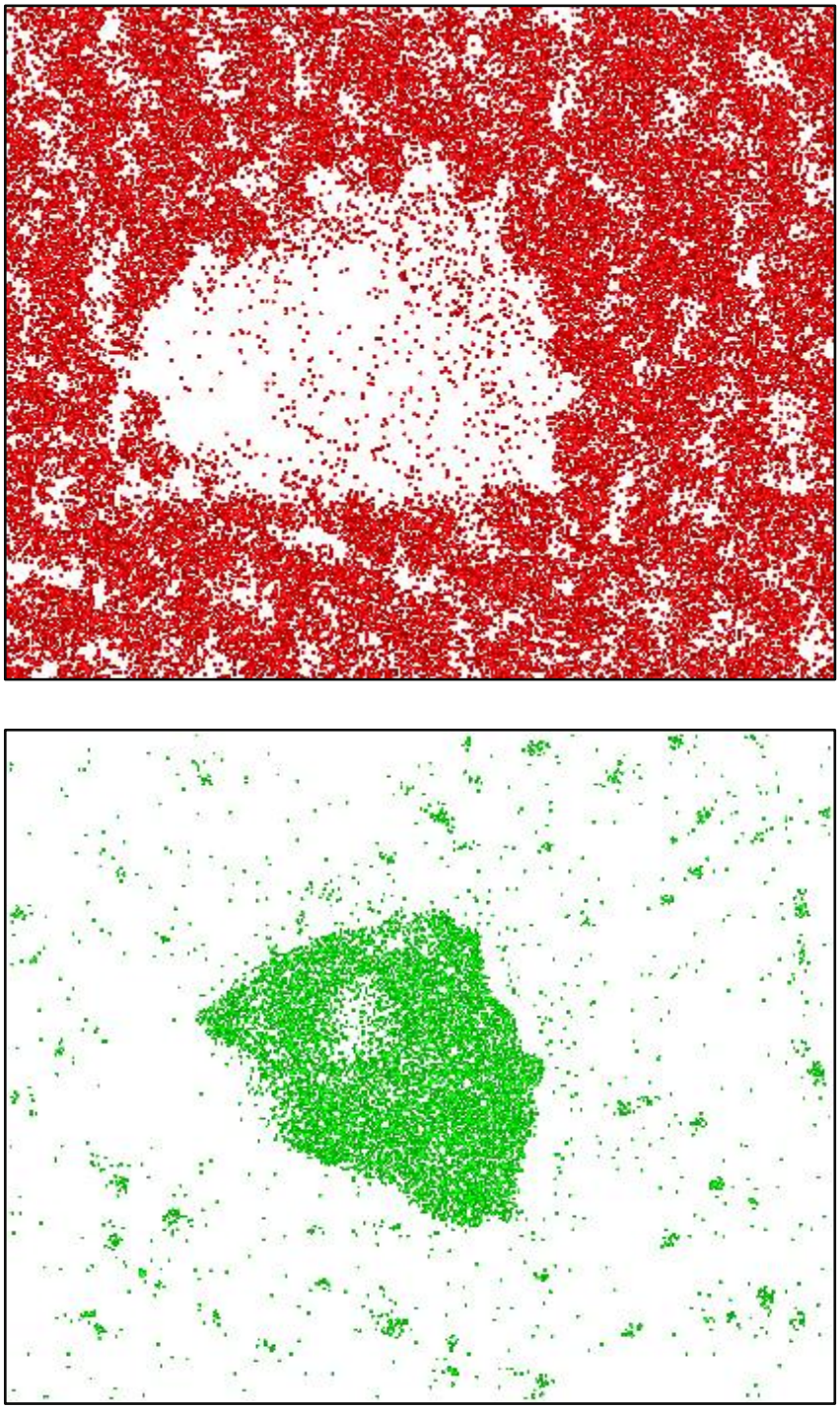

Figure 31 EDX analysis of a silicon particle included in the aluminum layer (red area showed in the picture above) and silicon particle (green area showed in the picture below).

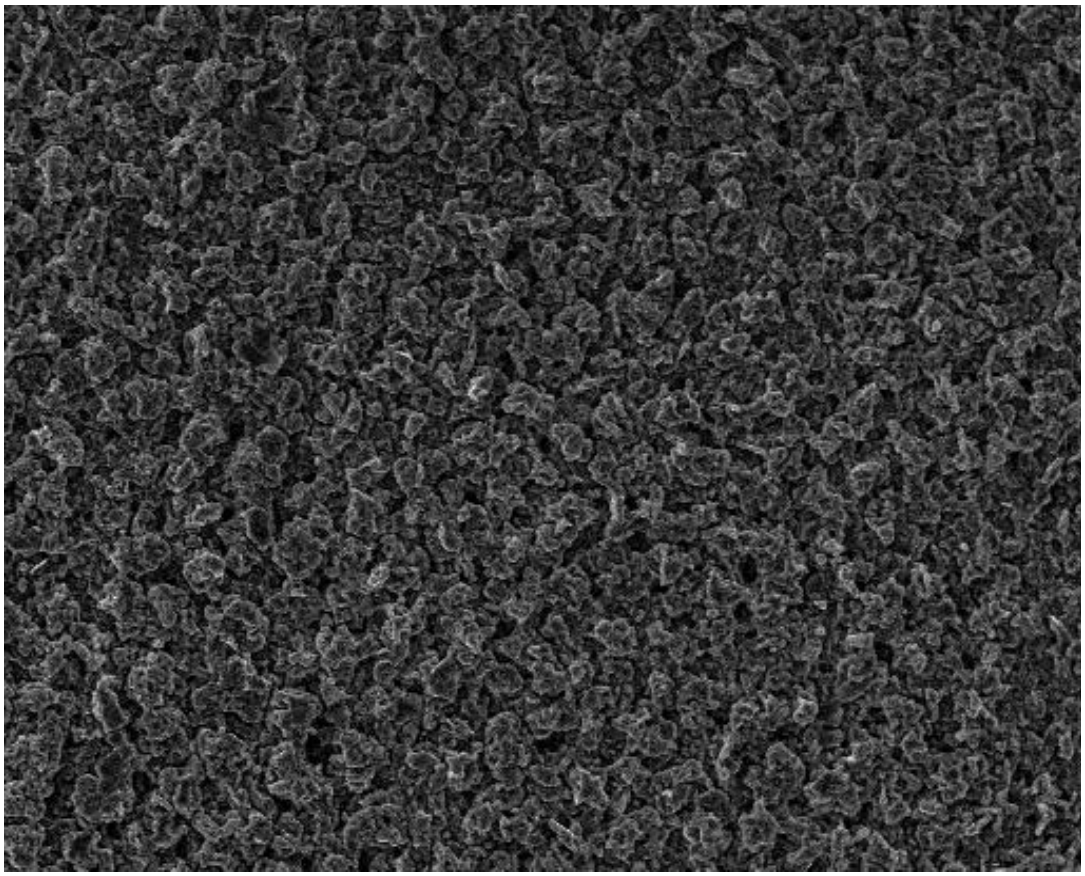

Figure 32 SEM micrograph of an Al-Si layer.

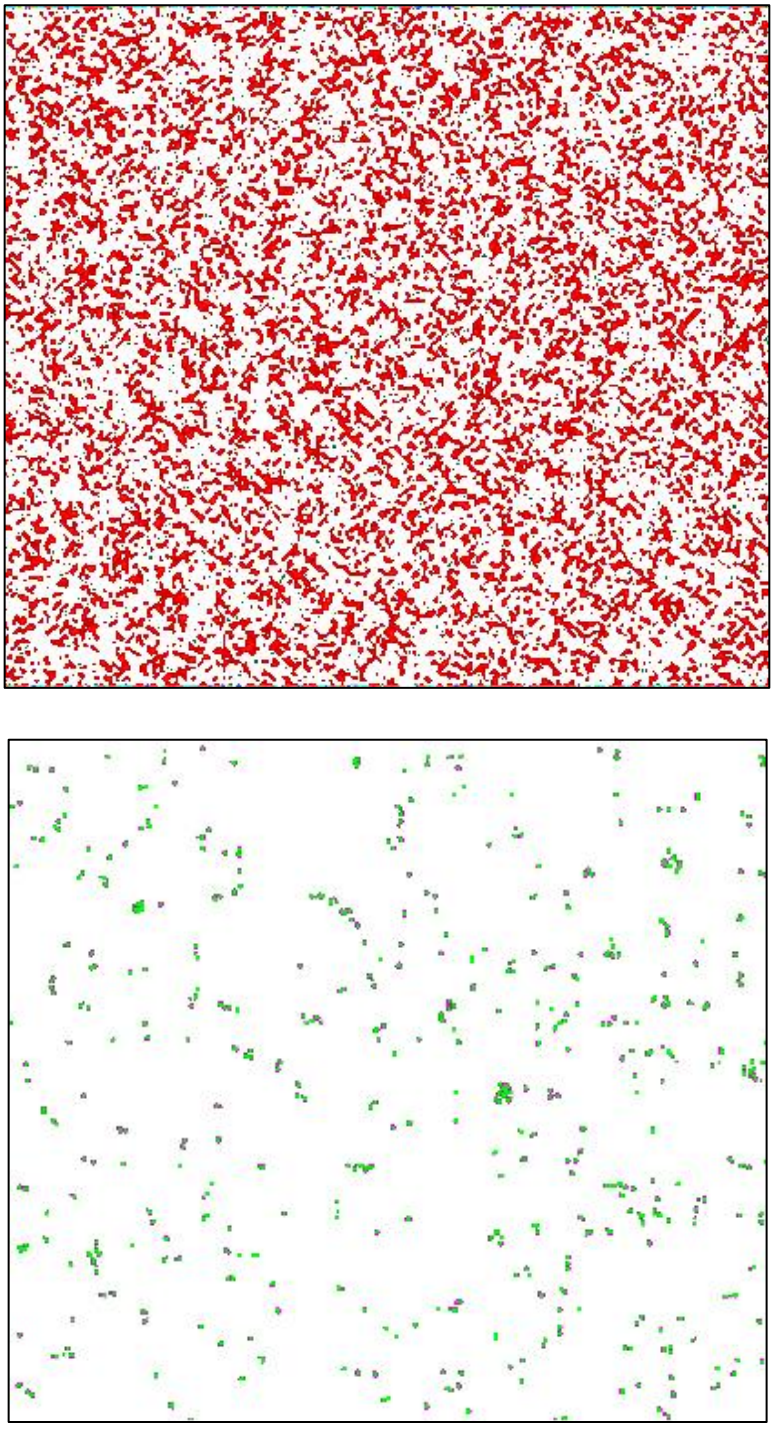

Figure 33 EDX analysis of an Al-Si layer, it detected aluminum crystals distribution (red area showed in the picture above) and silicon particles distribution on sample surface (green area showed in the picture below).

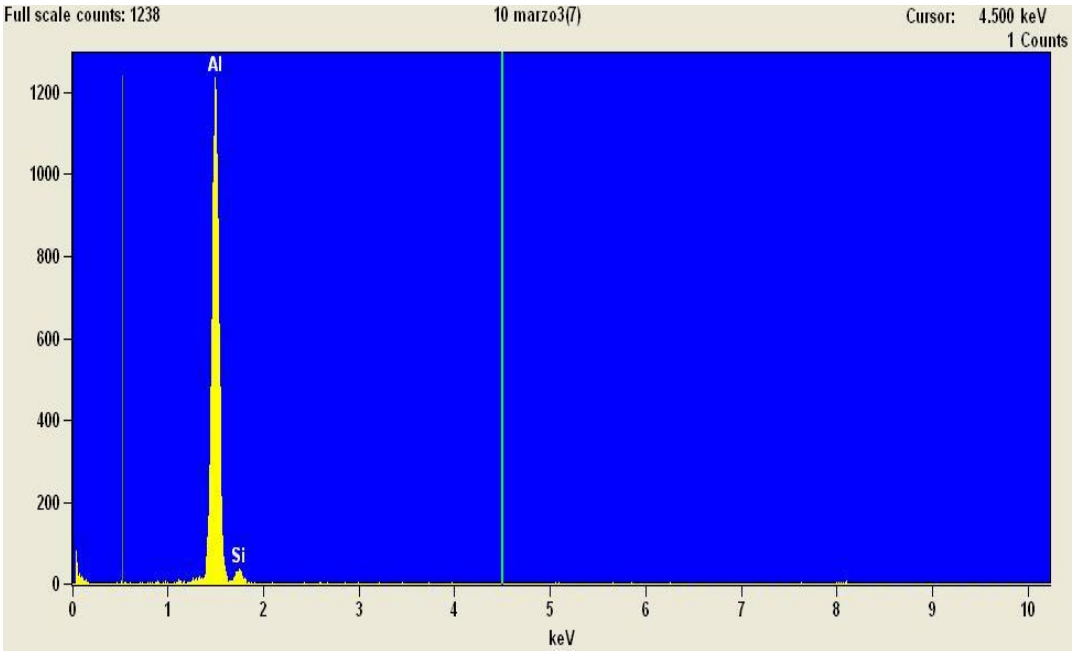

Figure 34 EDX report about the detection of metals in the layer. The higher peak corresponds to 93 wt % of aluminum and the small one to 7 wt % of silicon.

These results show the feasibility of the method for obtaining a composite layer of Al and Si. Tests on the actual suitability of this coating as way to protect superalloys from corrosion are in progress.

8 Electroless aluminum plating.

The previous lines of research follow the classical electroplating method, where a current is supplied to reduce aluminum anions ($Al_2Cl_7^-$) dissolved in the electrolyte (ionic liquid). Instead, the purpose of the third line of research focuses on the possibility to obtain aluminum coatings using electroless plating, where the aluminum reduction process occurs without supplying an external current. This process has some evident advantages over the electrodeposition process, in not requiring complex equipment, and also being able to coat complex shaped objects and even internal parts which are shielded from the electric field of an electrodeposition cell. This kind of approach is the equivalent of the well-known nickel electroless deposition process which has many industrial applications [95].

In literature, aluminum electroless plating is already known and it considers the decomposition of $AlH_3[O(C_4H_9)_2]$ using a catalyst treatment, by $Ti(O\text{-}i\text{-}Pr)_4$, of the substrate to accelerate the reaction rate . Other aluminum electroless procedures for preparation of Al films from [EMImCl] [$AlCl_3$] are known [96], [97]. In these cases aluminum electrodeposition is due to the reduction of $Al_2Cl_7^-$, which is the ionic species for aluminum deposit in the acidic [EMIm]Cl [$AlCl_3$] melt, by adding to the electrochemical bath LiH, $LiAlH_4$ and DIBAH (diisobutyl aluminum hydride) as reducing agents.

The present study is also based on using $LiAlH_4$ dissolved in ionic liquids. In this work aluminum deposition is not attempted by reduction of $Al_2Cl_7^-$, but by decomposition process of lithium aluminum hydride itself. In this way, even ionic liquids not containing $Al_2Cl_7^-$ can be employed.

In order to obtain the decomposition and the reduction of the dissolved aluminum, we observed that several studies have revealed important details about $LiAlH_4$ thermal decomposition behavior, [98]. The decomposition is expected to occur in a three-step process, although some controversy about the details of mechanism exist:

$LiAlH_4 \rightarrow \frac{1}{3}Li_3AlH_6 + \frac{2}{3}Al + H_2$ (I)

$\frac{1}{3}Li_3AlH_6 \rightarrow LiH + \frac{1}{3}Al + \frac{1}{2}H_2$ (II)

$LiH \rightarrow Li + \frac{1}{2}H_2$ (III)

By heating the solution, a spontaneous redox reaction occurs, where H^- undergoes an oxidation process and Al^{3+} the reduction, so metallic aluminum is obtained as reaction product. This reaction is therefore promising for the application sought here and has been object of extensive investigation in the present thesis work.

8.1 Experimental details.

Lithium aluminum hydride, $LiAlH_4$ (purity 95 % min), was supplied in pellet form by Aldrich. The pellets were pulverized by mortar and pestle operating in an inert atmosphere. $LiAlH_4$ 1.0 M in diethylether was supplied by Aldrich and it was used as received. The following ionic liquids were supplied by Merck and they were used as received, without further purification:

1) ethyl-dimethyl-propylammonium bis(trifluoro methyl sulfonyl)imide
2) 1-butyl-3-methylimidazolium trifluoromethanesulfonate
3) 1-hexyl-3-methylimidazolium tris(pentafluoroethyl)trifluorophosphate
4) 1-butyl-3-methylimidazolium hexafluorophosphate
5) 1-butyl-3-methylimidazolium tetrafluoroborate
6) 1-(3-methoxy propyl)-1-methyl-piperidine bis(trifluoromethylsulfonyl)imide
7) 1-butyl-3-methylpyrrolidinium bis(trifluoromethylsulfonyl)imide

All the experiments described in this section were conducted inside a glove box filled by nitrogen gas, to protect the ionic liquids from atmospheric moisture.

8.1.1 Experimental details about $LiAlH_4$ pellets in ethyl-dimethyl-propylammonium bis(trifluoro methyl sulfonyl)imide.

One $LiAlH_4$ pellet, weight equal to 1.666 g., was pulverized by mortar and pestle and added to 80 ml of ethyl-dimethyl-propylammonium bis(trifluoro methyl sulfonyl)imide, (Figure 35).

To carry out a systematic study of the solubility, the suspension was divided in 5 samples of

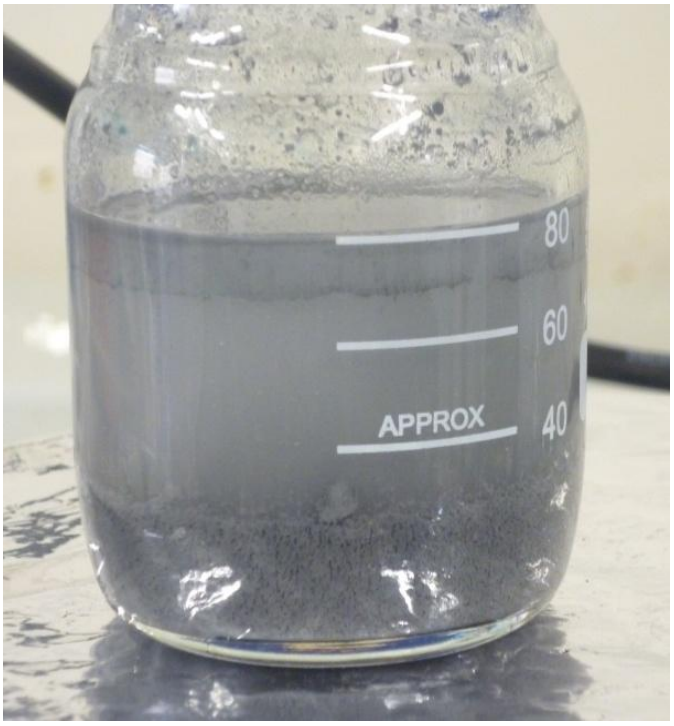

Figure 35 Suspension obtained adding 1.666 g of pulverized $LiAlH_4$ pellet to 80 ml of of ethyl-dimethyl-propylammonium bis(trifluoro methyl sulfonyl)imide.

15 ml and used in several stirring and thermal processes.

- Sample 1: simple suspension as obtained.
- Sample 2: under stirring for 24 hours at 25 °C.
- Sample 3: under stirring for 72 hours at 25 °C.
- Sample 4: under stirring for 120 hours at 25 °C.
- Sample 5: under stirring for 8 hours at 70 °C.

Except for the sample 1, after the treatment the suspension were filtered by Whatman paper filter n°6, because the viscosity of ionic liquid did not allow to carry out a decantation procedure of the suspension. Isothermal experiments were conducted on the five samples, setting the temperature for 1 hour in the range from 120°C to 170°C with 10°C intervals and using a copper foil as substrate. The copper substrates were investigated by scanning electron microscope and EDX analysis.

8.1.2 Experimental details about $LiAlH_4$ 1.0 M in diethylether in several ionic liquids.

The solubility of $LiAlH_4$ was tested using a solution of $LiAlH_4$ already dissolved in diethylether, in concentration equal to 1.0 molar. The low boiling point of diethylether (34.6 °C) allows a easy and fast elimination of this organic solvent by heating, after the addition to the ionic liquid. The solubility of $LiAlH_4$ 1.0 M in diethylether was tested by a systematic study in seven ionic liquids. For every ionic liquid two samples were prepared with two different concentrations of $LiAlH_4$, respectively 0.1 M and 0.01 M. The ionic liquids which showed a good solvation on $LiAlH_4$ were heated at 60 °C under stirring to remove diethylether and then they were investigated by isothermal processes to study the aluminum decomposition behavior on different substrates.

The temperature was setting for 1 hour at 160 °C and 175 °C and as substrates were used aluminum foil and wire and golden wire. The substrates were investigated by scanning electron microscope and EDX analysis.

8.2 Results and discussion.

Copper substrates which underwent electroless deposition were investigated by scanning electron microscope and EDX analysis. None showed detectable aluminum on the surface

except for one sample (sample 1) which showed a small amount of aluminum. Pulverized $LiAlH_4$ shows a low solubility in ethyl-dimethyl-propylammonium bis(trifluoro methyl sulfonyl)imide, so the amount of aluminum dissolved in the ionic liquid was not enough to obtain an aluminum deposit on the substrate. In fact, the only sample which showed a decomposition of aluminum was the suspension, where the concentration of aluminum was equal about to 1.0 M. For this reason we decided to focus the study on the investigation of solubility in several ionic liquids, and using $LiAlH_4$ already dissolved in an organic solvent (diethylether).

In order to test the solubility of $LiAlH_4$ 1.0 M in diethylether a systematic study was carried out. Two samples containing different concentrations of $LiAlH_4$ were prepared for every ionic liquid (the concentrations tested were 0.1 M and 0.001 M).

The results were summarized in 4, where

The numbers reported in the first row indicate the ionic liquids tested on the basis of the following list:

1) ethyl-dimethyl-propylammonium bis(trifluoro methyl sulfonyl)imide
2) 1-butyl-3-methylimidazolium trifluoromethanesulfonate
3) 1-hexyl-3-methylimidazolium tris(pentafluoroethyl)trifluorophosphate
4) 1-butyl-3-methylimidazolium hexafluorophosphate
5) 1-butyl-3-methylimidazolium tetrafluoroborate
6) 1-(3-methoxy propyl)-1-methyl-piperidine bis(trifluoromethylsulfonyl)imide
7) 1-butyl-3-methylpyrrolidinium trifluoromethansulfonate.

In the first column are reported the two concentrations, 0.1 M and 0.01 M respectively, of $LiAlH_4$, that I tested in every ionic liquid.

Red and black squares indicate the ability of $LiAlH_4$ to be dissolved in a ionic liquid and in a specific concentration:

✓ Red square means the ionic liquid showed a good solubility and it was investigated by isothermal experiments.

✓ Black square means the ionic liquid did not show a good solubility and it generated a two-phase system or a viscous compound.

	1	2	3	4	5	6	7
[0,01]	■	■	■	■	■	■	■
[0,1]	■	■	■	■	■	■	■

Table 4 Summary of the solubility tests conducted in 7 different ionic liquids, of $LiAlH_4$ 1.0 M in diethylether.

The ionic liquids where $LiAlH_4$ showed a good solubility are:

2) 1-butyl-3-methylimidazolium trifluoromethanesulfonate.

5) 1-butyl-3-methylimidazolium tetrafluoroborate.

7) 1-butyl-3-methylpyrrolidinium trifluoromethansulfonate.

8.2.1 Decomposition reaction in 1-butyl-3-methylimidazolium trifluoromethanesulfonate.

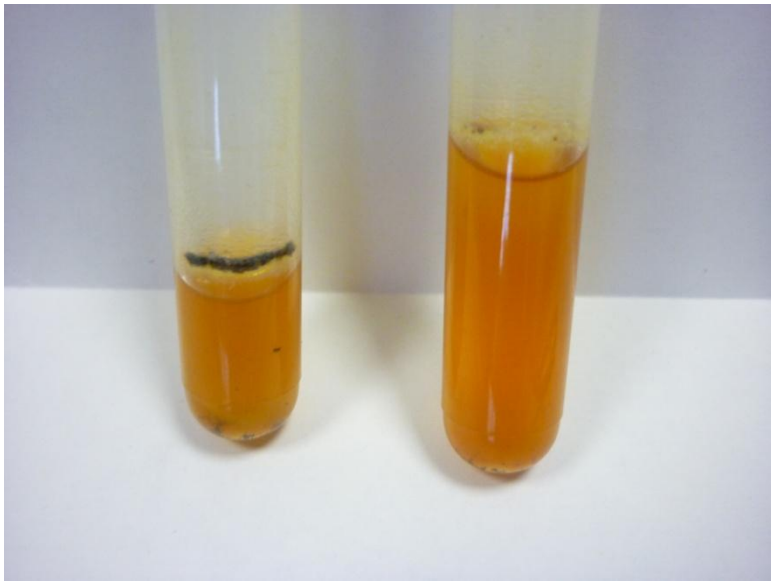

Figure 36 Solubility tests conducted in 1-butyl-3-methylimidazolium trifluoromethanesulfonate, of $LiAlH_4$ 1.0 M in diethylether. On the left side the sample 0.1 M in $LiAlH_4$, on the right the sample 0.001 M in $LiAlH_4$.

Adding $LiAlH_4$ 1.0 M in diethylether to the ionic liquid, a black precipitate was formed. It was extracted from ionic liquid by dichloromethane and then filtered by Whatman paper filter n°6. The fine powder was investigated by SEM-EDX and it identified the powder as metallic aluminum crystals.

In order to carry out a gravimetric analysis of the process, 20 ml of 1-butyl-3-methylimidazolium trifluoromethanesulfonate 0.1 M in $LiAlH_4$ was prepared, so 2 mmol of aluminum (equal to 26 mg) were solvate by the ionic liquid. The metallic aluminum powder extracted from the solution was equal to 6.54 mg, that means the 25.15 % of aluminum present in the solution underwent the decomposition process. Figure 37 shows the morphology and composition analyses effectuated on aluminum particles. Crystals are characterized by a size range from 10 to 25 μm.

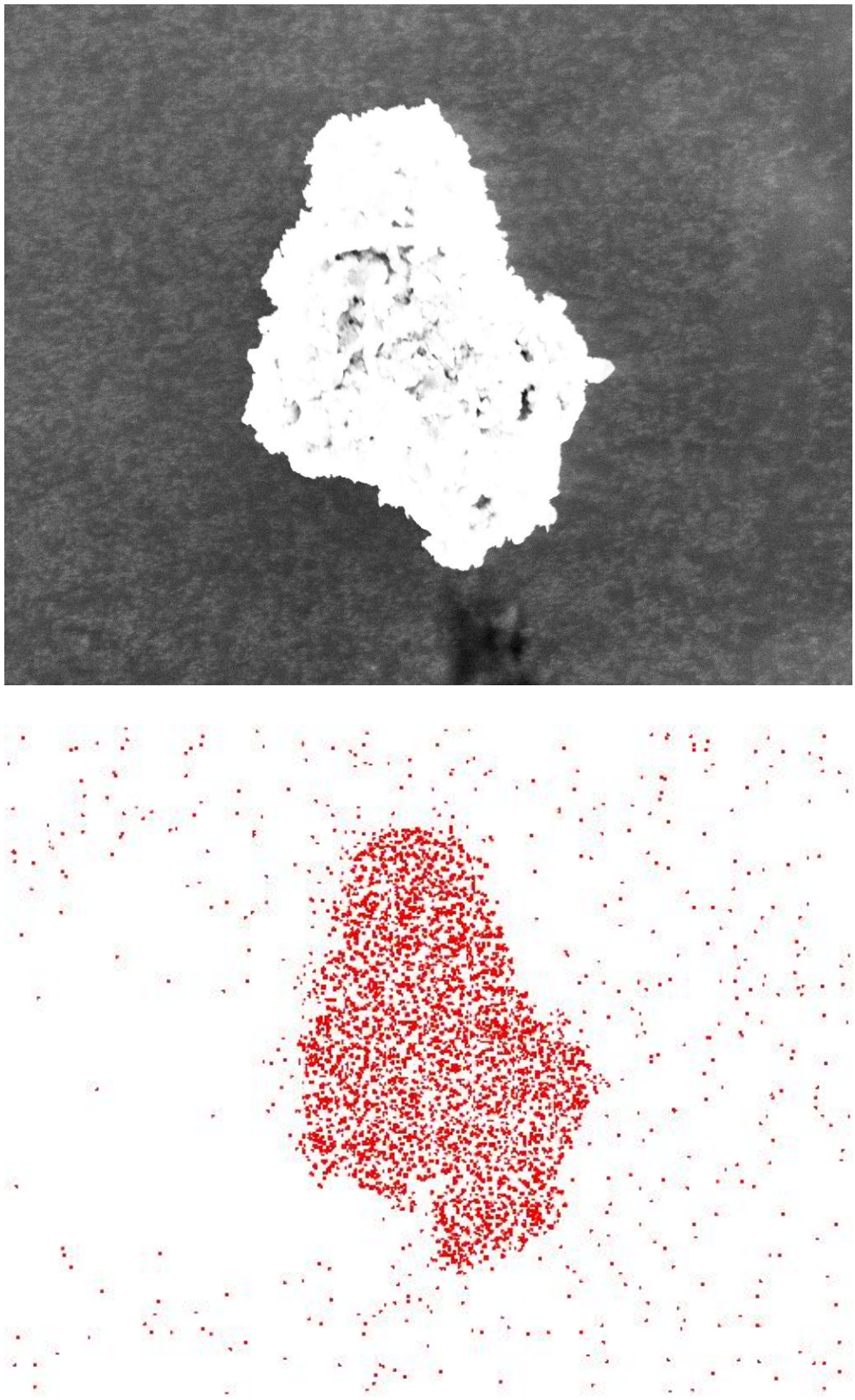

Figure 37 SEM micrograph of a precipitated particle. EDX analysis showed aluminum presence as red points.

In order to verify the influence of temperature on the process, a series of isothermal experiments were conducted on the solutions for 1 hour, increasing the temperature from 170°C to 250°C at 10°C intervals. Aluminum wire and gold wire were introduced in the solution to check the affinity of aluminum crystals to these two different substrates and if they adhere to them. The experiments showed that temperature did not enhance the decomposition process and the gravimetric analyses evidenced a percentage of metallic aluminum equal to about 25 %. Aluminum crystals did not manifest any affinity for the substrates and they were still precipitated as fine powder on the bottom of the beaker.

8.2.2 Solubility estimation in 1-butyl-3-methylimidazolium tetrafluoroborate.

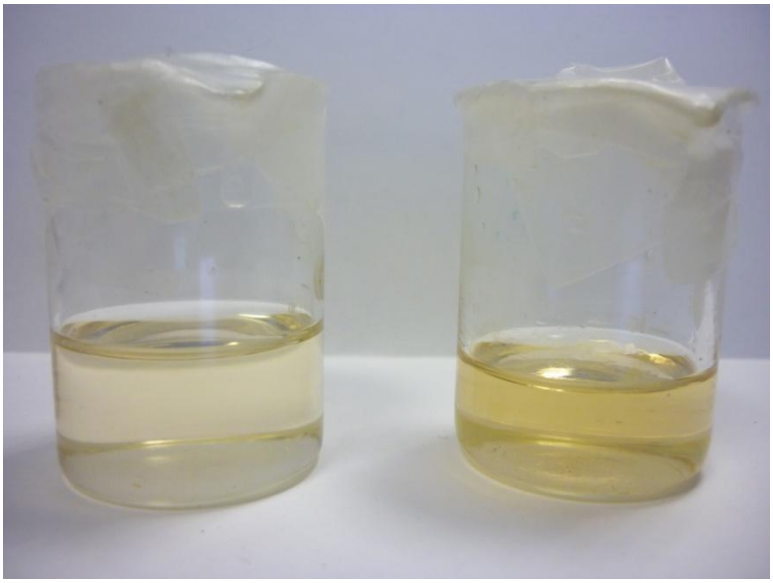

Figure 38 Solubility tests conducted in 1-butyl-3-methylimidazolium tetrafluoroborate, of $LiAlH_4$ 1.0 M in diethylether. On the left side the sample 0.01 M in $LiAlH_4$, on the right the sample 0.001 M in $LiAlH_4$.

Preparing 20 ml of 1-butyl-3-methylimidazolium tetrafluoroborate 0.01 M in $LiAlH_4$, a suspension of white particles were observed in the ionic liquid and they were still present after 2 hours under stirring. Because of too low solubility of $LiAlH_4$ in [BMIm] [BF_4], at room temperature, it is difficult to estimate it using this small volume of ionic liquid. For this reason I decided to heat the solution until the corpuscles were dissolved in the solvent, in order to discovery at which temperature this amount of hydride is soluble in [BMIm] [BF_4].

The particles disappeared at 160 °C, so knowing [BMIm] [BF_4] density (1.21 g/ml) I could easily calculate:

0.017 g of $LiALH_4$ for 100 g of [BMIm] [BF_4] at 160 °C.

8.2.3 Solubility estimation in 1-butyl-3-methylpyrrolidinium bis(trifluoromethansulfonate).

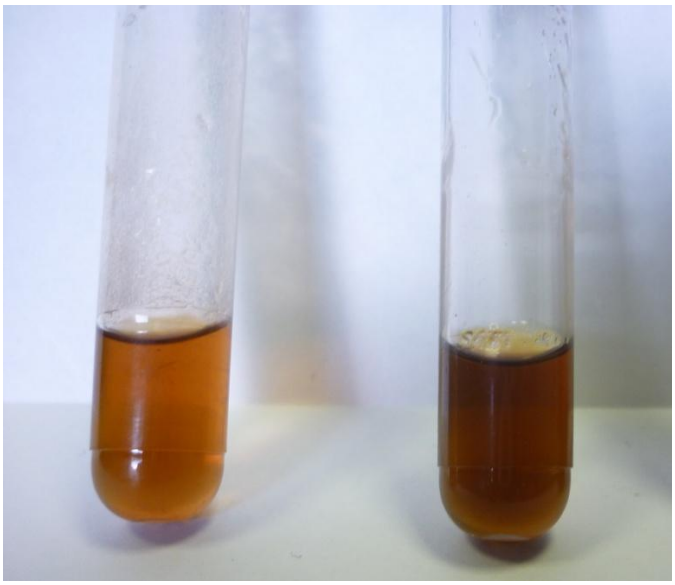

Figure 39 Solubility tests conducted in 1-butyl-3-methylpyrrolidinium bis(trifluoromethansulfonate), of $LiAlH_4$ 1.0 M in diethylether. On the left side the sample 0.1 M in $LiAlH_4$, on the right the sample 0.001 M in $LiAlH_4$.

A 20 ml sample of 1-butyl-3-methylpyrrolidinium bis(trifluoromethansulfonate) 0.01 M in $LiAlH_4$ did not present any solid corpuscles, so that means the solubility, even at room temperature, is higher. In order to estimate the solubility value, a constant volumes of $LiAlH_4$ 1.0 M in diethylether equal to 0.02 ml have been added to the solution step by step, to identify at which concentration $LiALH_4$ starts to precipitate.

At room temperature, a solid particulate was observed in the solution after the addition of 0.06 ml of $LiAlH_4$ 1.0 M in diethylether. Heating the suspension just few minutes at 40 °C is enough to dissolve the particles and get the solution again. Being [BMPL] [OTF] density equal to 1.25 g/ml, the solubility is:

0.026 g of $LiALH_4$ for 100 g of [BMPL] [OTF] at 40 °C.

8.2.4 Isothermal experiments.

In another set of experiments, 20 ml of 1-butyl-3-methylpyrrolidinium bis(trifluoromethansulfonate 0.01 M in $LiAlH_4$ and 20 ml of 1-butyl-3-methylimidazolium tetrafluoroborate 0.01 M in $LiAlH_4$ were prepared. A series of isothermal experiments were conducted on the solutions, using as substrate aluminum wire and gold wire (Figure 40), setting the temperature for 1 hour in the range from 170°C to 250°C with 10°C intervals.

Temperatures higher than 250 °C were not tested, because these ionic liquids undergo a

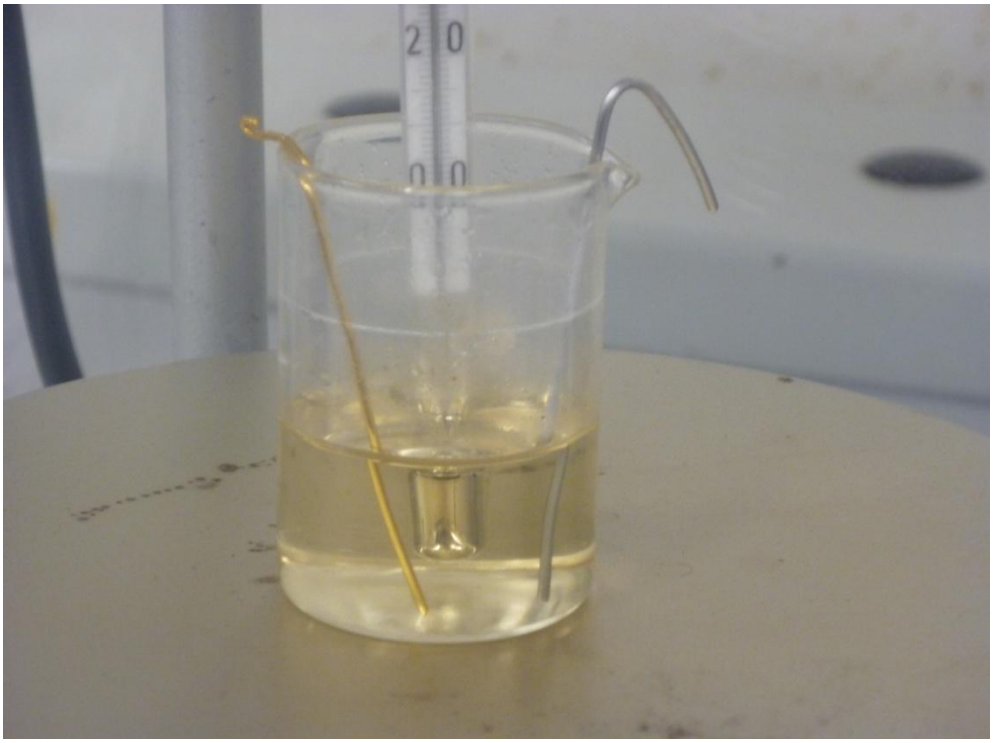

Figure 40 Isothermal experiment conducted for 1 hour on 1-butyl-3-methylpyrrolidinium bis(trifluoromethansulfonate) 0.01 M in $LiAlH_4$ using as substrate aluminum wire and gold wire.

decomposition process at about 300 °C [99]. These experiments proved that the decomposition of $LiAlH_4$ is not promoted by temperature. An explanation could be connected to complex ions formed between $LiAlH_4$ and ionic liquids during the hydride dissolution. These complexes likely have a stable structure that impedes the mechanism of decomposition of $LiAlH_4$. In the experiments conducted using 1-butyl-3-methylimidazolium trifluoromethanesulfonate, the decomposition process was spontaneous and it started even without supplying heat, because the interaction between hydride and ionic liquid does not

produce any complex ions and it brings directly to the decomposition process. This set of experiments has to be considered as still preliminary. Although it was not possible to obtain the formation of aluminum films on the substrates tested, they show at least that it is possible to obtain the reduction of $LiAlH_4$ dissolved in ionic liquids, obtaining aluminum in metallic form. Further experiments are necessary to determine if specific combinations of solvent and substrate will make it possible to obtain aluminum films of industrial interest.

9 Conclusion.

This work covered the field of ionic liquid as media for aluminum electrodeposition and for aluminum electroless plating. The first line of research showed that it is possible to significantly influence the electrodeposition of aluminum by the addition of six organic compounds. The electrochemical investigations demonstrated that a temperature increase (from 25 °C to 100 °C) influences the reaction rate, which becomes faster because of the increased charge transfer and mobility of the electroactive species towards the electrode surface. Moreover, they showed the adsorption of the additives determines a deposition overpotential increase, which affects the nucleation activation energy by means of these additives, nanocrystalline, shiny aluminum layers can be electrodeposited adding the different organic compounds to the ionic liquid and in particularly adding 2-chloro nicotinic acid and 1-methoxy naphthalene, in addition to the bright and shiny characteristics the coatings show even a particular and interesting goldish coloring.

A new technique to perform aluminum electrodeposition out of the glove box was tested using a nozzle submerged in the ionic liquid which pumps an inert gas inside the bath. The system was tested by constant potential depositions that were generated from [EMIm]Cl/$AlCl_3$ with the addition of 2-chloro nicotinic acid at 25 °C. The coatings obtained using this innovative technique are uniform with a very fine crystallites in the nanometer regime and, as the deposits realized inside glove box, they show a goldish shining surface. The good results obtained by this novel method to realize aluminum coatings out of the glove box prompts to further studies of this procedure in order to improve the system and to employ it for applications not just in experimental stage.

The study aimed at creating aluminum-silicon coatings by electrodeposition demonstrated that a homogeneous suspension has a fundamental importance to get aluminum layers containing an uniform distribution of silicon. The study has showed that silicon particles can be included in aluminum deposits if the ratio of silicon to aluminum grains size is smaller then 10^2, whereas the silicon concentration in the electrochemical bath influences its percentage in the coatings. With appropriate parameters, it is possible to obtain aluminum layer containing a uniform distribution of about 7 % in weight of silicon particles embedded

in the layer. This process is of particular interest because Al-Si coatings are a potential substitute of the layers obtained by chromatization. So, further studies can be focused on this topic in order to develop a scale-up of the procedure and replace the old and dangerous technology.

The last line of research focused on the possibility to obtain aluminum coatings using electroless plating. It is based on using $LiAlH_4$ in different ionic liquids and carrying out isothermal experiments. These tests showed the possibility of dissolving and reducing $LiAlH_4$ in ionic liquids, but did not produce a layer of metallic aluminum. The phenomenon is likely connected to complexes that $LiAlH_4$ forms in the ionic liquids, which have a stable structure that impedes the mechanism of decomposition and causes aluminum to precipitate as powder. Although depositing Al layers turned out to be impossible in the conditions tested here, this series of experiments show promise and are being further pursued.

Summarizing, the main innovations resulting from this thesis work can be listed as:

1. Demonstration of the possibility of using organic precursors to obtain shiny, nanocrystalline aluminum layers by electrodeposition from ionic liquids

2. Demonstration of the possibility of carrying out aluminum electrodeposition from ILs in simplified experimental conditions, using the bubbling of argon in the deposition bath to eliminate the hygroscopicity problem

3. Demonstration of the possibility of obtaining a composite Al-Si coating with up to 7 % Si concentration by means of electrodeposition from ILs containing a suspension of Si particles

4. Attempt at the electroless deposition of aluminum layer by decomposition of an aluminum salt dissolved in ionic liquid.

10 Bibliography.

[1] http://www.laboratory-journal.com.

[2]I. Yavari, E. Kowsari, Tetrah. Lett. 48 (2007) 3753.

[3]L.C. Branco, C.A.M. Afonso, Tetrah. Lett. 57 (2001) 4405.

[4]Y. Tsukada, K. Iwamoto, H. Furutani, Y. Matsushita, Tetrah. Lett. 47 (2006) 1801.

[5]P. Cserjési, N. Nemestóthy, A. Vass, Zs. Csanádi, K. Bélafi-Bakó, Desalin. 24 (2009) 743.

[6]M. Baghdadi, F. Shemirani, Anal. Chim. Act. 634 (2009) 186.

[7]T. Joseph, S. Sahoo, S.B. Halligudi, J. Molec. Catal. 234 (2005) 107.

[8]G. Cheruvally, J.K. Kim, J.W. Choi, J.H. Ahn,, J. Pow. Sou. 172 (2007) 863.

[9]H. Wang, Q. Lu, C. Ye, W. Liu, Z. Cui, Wear 256 (2004) 44.

[10]A. Hernández Battez, R. González, J.L. Viesca, D. Blanco, Wear 266 (2009) 1224.

[11]A.E. Jiménez, M.D. Bermúdez, F.J. Carrión, G. Martínez-Nicolás, Wear 261 (2006) 347.

[12]H. Kamimura, T. Kubo, I. Minami, S. Mori, Trib. Int. 40 (2007) 620.

[13]M.D. Bermudez, A.E. Jimenez, J. Sanes, F.J. Carrion, Molec. 14 (2009) 2888.

[14]A.P. Abbott, C.A. Eardley, N.R.S. Faley, G.A. Griffith, J. Appl. Electrochem. 31 (2001) 1345.

[15]Q. Liao, W.R. Pitner, G. Stewart, C.L. Hussey, J. Electrochem. Soc. 144 (1997) 133.

[16]R.T. Carlin, W. Crawford, M. Bersch, J. Electrochem. Soc. 139 (1992) 2720.

[17]P.K. Lai, M.S. Kazacos, J. Electroanal. Chem. 248 (1988) 431.

[18]C. Suryanarayana, Int. Mater. Rev. 40 (1995) 41.

[19]F. Endres, ChemPhysChem 3 (2002) 144.

[20]P. Walden, Bull. Acad. Imper. Sci. (1914) 1800.

[21]F.H. Hurley, T.P.Wier, J. Electrochem. Soc. 98 (1951) 203.

[22]F.H. Hurley, T.P.Wier, J. Electrochem. Soc. 98 (1951) 207.

[23]R.J. Gale, B. Gilbert, R. A. Osteryoung, Inorg. Chem. 17 (1978) 2728.

[24]S. Takahashi, N. Koura, M.-L. Saboungi, L.A. Curtiss, Plasm. & Ions 2 (1999) 91.

[25]V.R. Koch, L.l. Miller, R.A. Ostreyoung, J. Am. Chem. Soc. 98 (1976) 5277.

[26]Y. Chauvin, A. Hirschauer, H. Olvier, J. Mol. Cat. 92 (194) 155.

[27]C.W. Lee, Tetrah. Lett. 40 (1999) 2461.

[28]R.T. Carlin, J.S. Wilkes, J. Mol. Cat. 63 (1990) 125.

[29]J.S. Wilkes, M.J. Zaworotko, J. Chem. Soc. Chem. Comm. 13 (1992) 965.

[30]R.D. Rogers, K. Seddon, Ionic Liquids as a Green Solvents, ACS Symp. Ser. 856 (2003).

[31]P. Bonhote, A.P. Dias, N. Papageorgiou, K. Kalyanasundaram, Inorg. Chem. 35 (1996) 1168.

[32]M.C. Buzzeo, R.G. Ewans, R.G. Compton, ChemPhysChem 5 (2004) 1106.

[33]H. Mizuuchi, V. Jaitely, S. Murdan, A.T. Florence, Eur. J. Pharm. Sci. 33 (2008) 326.

[34]J. H Jr. Davis, Chem. Lett. 33 (2004) 1072.

[35]L. Hussey, T.B. Scheffler, J.S. Wilkes, A.A. Fannin, J. Electrochem. Soc. 133 (1986) 1389.

[36]H.A. Øye, M. Jagton, T. Oksfjell, J.S. Wiles, Mat. Scien. For. 73 (1991) 183.

[37]M. Galinski, A. Lewandowski, I. Stepniak, Electrochim. Act. 51 (2006) 5567.

[38]P. Wasserscheid, T. Welton, “Ionic Liquids in Synthesis” Wiley-VCH (2003).

[39]H.L Ngo, K. LeCompte, L.Harges, A.B. McEwen, Thermochim. Act 357 (2000) 97.

[40]S.V Dzyuba, R.A.Bartsch. ChemPhysChem 3 (2002) 161.

[41]S.Seki, T. Kobayashi, Y. Kobayashi, K. Takei, H. Miyashiro, J. Mol. Liq. 152 (2010) 9.

[42]Z.B. Zhou, H. Matsumoto, K. Tatsumi, Chem. Eur. J. 12 (2006) 2196.

[43]O.O. Okoturo, T.J. VanderNoot, J. Electroanal. Chem. 568 (2004) 167.

[44]D.R. MacFerlane, J. Sun, J. Golding, P. Meakin, M. Forsyth, Electrochem. Act. 45 (2000) 1271.

[45]http://look4chemistry.blogspot.it/

[46]http://www.cheng.cam.ac.uk/

[47]http://www.garmanage.com/

[48]A. Ashok, P. Pal, The Scient. World J. 2014 (2014) 9.

[49]http://cmrf.research.uiowa.edu/

[50]http://www.porous-35.com/

[51]J. Bard, L.R. Faulkner, Electrochemical methods J. Wiley & Sons (2001).

[52]http://www.expertsmind.com/

[53]T.P. Moffat, J. Electrochem. Soc. 141 (1994) 115.

[54]G.R. Stafford, J. Electrochem. Soc. 136 (1989) 635.

[55]T.P. Moffat, J. Electrochem. Soc. 141 (1994) 3059.

[56]G.M.Janowski, G.R. Stafford, Met. Trans. 23 (1992) 2715.

[57]R.A. Carpio, L.A. King, R.E. Lindstrom, J.C. Nardi, J. Electrochem. Soc. 126 (1979) 1644.

[58]A.A. Fannin Jr., D.A. Floreani, L.A. King, S.S. Ianders, J. Phys. Chem. 88 (1984) 2614.

[59]J.S. Wilkes, J.A. Levisky, R.A. Wilson, C. Hussey, Inorg. Chem. 21 (1982) 1263.

[60]Y.Zhao, T.J. VanderNoot, Electrochim. Act. 42 (1997) 3.

[61]UNI ISO 9227, (1993).

[62]C. Suryanarayana, F.H. Froes, Metall Trans 23A (1992) 1071.

[63]M.A. Meyers, A. Mishra, D.J. Benson, Prog. Mater. Sci. 51 (2006) 427.

[64]M. A. Alodan, W. H. Smyrl, Electrochim. Act. 44 (1998) 299.

[65]F. Lallemand, L. Ricq, P. Berçot, J. Pagetti, Electrochim. Act. 47 (2002) 4149.

[66]L. Ricq, F. Lallemand, M. P. Gigandet, J. Pagetti, Surf. Coat. Techn. 138 (2001) 278.

[67]T. Osaka, T. Sawaguchi, F. Mizutani, J. Electrochem. Soc. 146 (1999) 3295.

[68]A. Bouyaghroumni, P. Versaud, Can. Metall. Q. 35 (1996), 245.

[69]I. Tabakovic and S. Riemer, J. Electrochem. Soc. 147 (2000) 219.

[70]Y.-Li. Zhu, Y. Kozuma, Y. Katayama, T. Miura, Electrochim. Act. 54 (2009) 7502.

[71]L. Oniciu, L.Muresan, J. Appl. Electrochem. 21 (1991) 565.

[72]N. Eliaz, G. Shemesh, R.M. Latanision, Engin. Fail. Anal. 9 (2002) 31.

[73]http://hghouston.com/

[74]G.Y. Lai, High Temperature Corrosion and Materials Applications ASM (2007).

[75]C.H. Lund, H.J. Wagner, Def. Met. Infor. Cent. 214 (1965).

[76]N. Dulcy, M. Sc. Thesis, Cranfield University – School of Applied Physics (2007) 13.

[77]J.R. Nicholls, N.J. Simms, W.Y. Chan, E.H. Evans, Surf. and Coat. Techn. 149 (2002) 236.

[78]N. Eliaz, G. Shemesh, R.M. Latanison, Engineering Failure Analysis 9 (2002) 31.

[79]M.J. Pomeroy, Materials & Design 26 (2005) 223.

[80]P. Box, M. Whitehurst, UK patent GB 2421032 (2006).

[81]P.M. Walker, M.F. Whitehurst, UK patent GB 249313 (2007).

[82]E. Godlewska, K. Godlewski, Oxidat. Of Met. 22 (1984) 117.

[83]M.C. Meelu, UK patent GB 2322382 (1998).

[84]R. Mobarra, A.H. Jafari, M. Karaminezhaad, Surf. and Coat. Techn. 201 (2006) 2002.

[85]I. Gurrappa, Surf. and Coat. Techn. 139 (2001) 27.

[86]P.K. Datta, J.S. Burnel-Gray, K. Natesan, Intermetal. Comp. Princ. And Pract. III (2002) 561.

[87]M.C. Meelu, Materials & Design 14 (1993) 53.

[88]T.S. Sidhu, S. Prakash, RD. Agrawal, Scripta Materialia 55 (2006) 179.

[89]J.M. Guilemany, J. Fernandez, J. Delgado, Surf. and Coat. Techn. 153 (2002) 107.

[90]Z.D. Xiang, P.K. Data, Materials science and engineering 356 (2003) 136.

[91]B.R. Rose, P.R. Lavery, European patent EP0654542 (1995).

[92]B. McMordie, T.A. Kircher, European patent EP07483394 (1996).

[93]G.T. Bayer, K.A. Wynns, US patent application 20060222879 (2006).

[94]J. Kohlscheen, H.R. Stock, Surf. and Coat. Techn. 203 (2008) 476.

[95]H.M. Lee, S.Y. Choi, A. Jung, ACS Appl. Mat. & Interf. 5 (2013) 4581.

[96]N. Koura, H. Nagase, A. Sato, et al., J. Of the Electrochem. Soc. 155 (2008) D155.

[97]I. Shitanda, A. Sato, M. Itagaki, Electrochim. Act. 54 (2009) 5889.

[98]A. Andereasen, T. Vegge, A.S. Pedersen, J. Of Solid State Chem. 178 (2005) 3672.

[99]C. Maton, N. De Vos, C.V. Stevens, Chem. Soc. Rev. 42 (2013) 5963.